Thermodynamic properties of minerals and fluids

Eremin O.V.[1], Epova E.S.[1], Rusal O.S.[1], Bychinskii V.A.[2] Calculation of standard thermodynamic potentials of Cs-zeolites

[1] Institute of natural resources, ecology and cryollogy SB RAS, Chita

[2] Institute of geochemistry SB RAS, Irkutsk (yeroleg@yandex.ru)

Abstract. On the basis of thermodynamic properties of natural pollucite (Ogorodova et., al, 2003) the linear decomposition of the values of standard Gibbs energies and enthalpies of formation from the chemical elements have been obtained. Comparison of calculations with the literature data gives the estimation errors in the range of 0-6 %. The equation obtained for oxide increments can be used for assessments of the potential of zeolites in the Cs-Rb-Na-Al-Si-O-H system.

Keywords: Standard thermodynamic potentials, Cs-zeolites.

Pollucite - $(Cs,Rb,Na)[AlSi_2O_6]\cdot nH_2O$ - is the only cesium-containing natural zeolite which represents the main ore mineral of cesium. The zeolites due to its ion-exchange capacity may include in their structures the cations of cesium. This property is actively studied in the sequestration of radioactive isotopes using natural and synthetic zeolites (Vipin et al., 2016; Brundu and Cerri, 2015).

On the base of thermodynamic properties of pollucite – $Cs_{0.77}Rb_{0.04}Na_{0.14}[Al_{0.91}Si_{2.08}O_6]\cdot 0.34H_2O$ determined by (Ogorodova et al., 2003) the linear decomposition of oxides increments for standard enthalpies and Gibbs energies have been calculated by mean of linear programming problems (Eremin, 2014; Eremin et al., 2016). The results presented in table 1. The comparison of calculated values with literature data presented in tables 2, 3. The obtained decompositions can be used for calculations of zeolites potentials of Cs-Rb-Na-Al-Si-O-H system.

Table 1. The values of Gibbs energies (G) and enthalpies (H) of pollucite $Cs_{0.77}Rb_{0.04}Na_{0.14}[Al_{0.91}Si_{2.08}O_6]\cdot 0.34H_2O$ from consisting oxides increments

y*, kJ/mole	Cs_2O	Rb_2O	Na_2O	Al_2O_3	SiO_2	H_2O
-H	411.959	733.131	663.954	1785.908	936.399	364.581
-G	378.879	678.289	619.521	1695.342	884.811	312.978

Table 2. The standard enthalpies of formation from the elements Cs-zeolites

Minerals	-H, kJ/mole	Calc.	Error, %
Pollucite $Cs_{0.77}Rb_{0.04}Na_{0.14}[Al_{0.91}Si_{2.08}O_6]\cdot 0.34H_2O$ (Ogorodova et al., 2003)	3104.000	3104.000	0.00
Pollucite $Cs_{0.65}Na_{0.185}Rb_{0.028}AlSi_2O_{5.863}(OH)_{0.32}\cdot 0.19H_2O$ (See references from Ogorodova et al., 2003)	3098.500	3098.922	-0.01
Pollucite (synth.) $CsAlSi_2O_6$ (See references from Ogorodova et al., 2003)	3083.400	2971.732	3.68
Pollucite $Cs_{0.84}Na_{0.11}Al_{0.88}Si_{2.1}O_6\cdot 0.17H_2O$ (Ogorodova et al., 2003)	3090.000	3023.757	2.17
Rb-Natrolite $Rb_{0.384}Al_{0.461}Si_{0.558}O_2(H_2O)_{0.42}$ (Wu et al., 2013)	1151.860	1228.048	-6.40
Rb-Beta H(0.0018)Na(0.005)Rb(0.05869)Al(0.06552)Si(0.93448)O2 (Sun et al., 2006)	912.630	956.372	-4.68
Cs-Beta H(0.0093)Na(0.005)Cs(0.05358)Al(0.06788)Si(0.93212)O2 (Sun et al., 2006)	909.620	958.204	-5.20

Table 3. The standard Gibbs energies of Cs-zeolites

Minerals	-G, kJ/mole	Calculated	Error, %
Pollucite $Cs_{0.77}Rb_{0.04}Na_{0.14}[Al_{0.91}Si_{2.08}O_6]\cdot 0.34H_2O$ (Ogorodova et al., 2003)	2921.000	2921.000	0.00
Pollucite $Cs_{0.65}Na_{0.185}Rb_{0.028}AlSi_2O_{5.863}(OH)_{0.32}\cdot 0.19H_2O$ (See references from Ogorodova et al., 2003)	2921.600	2916.772	0.17
Pollucite (synth.) $CsAlSi_2O_6$ (See references from Ogorodova et al., 2003)	2917.000	2806.732	3.85
Pollucite $Cs_{0.84}Na_{0.11}Al_{0.88}Si_{2.1}O_6\cdot 0.17H_2O$ (Ogorodova et al., 2003)	2911.000	2850.462	2.10

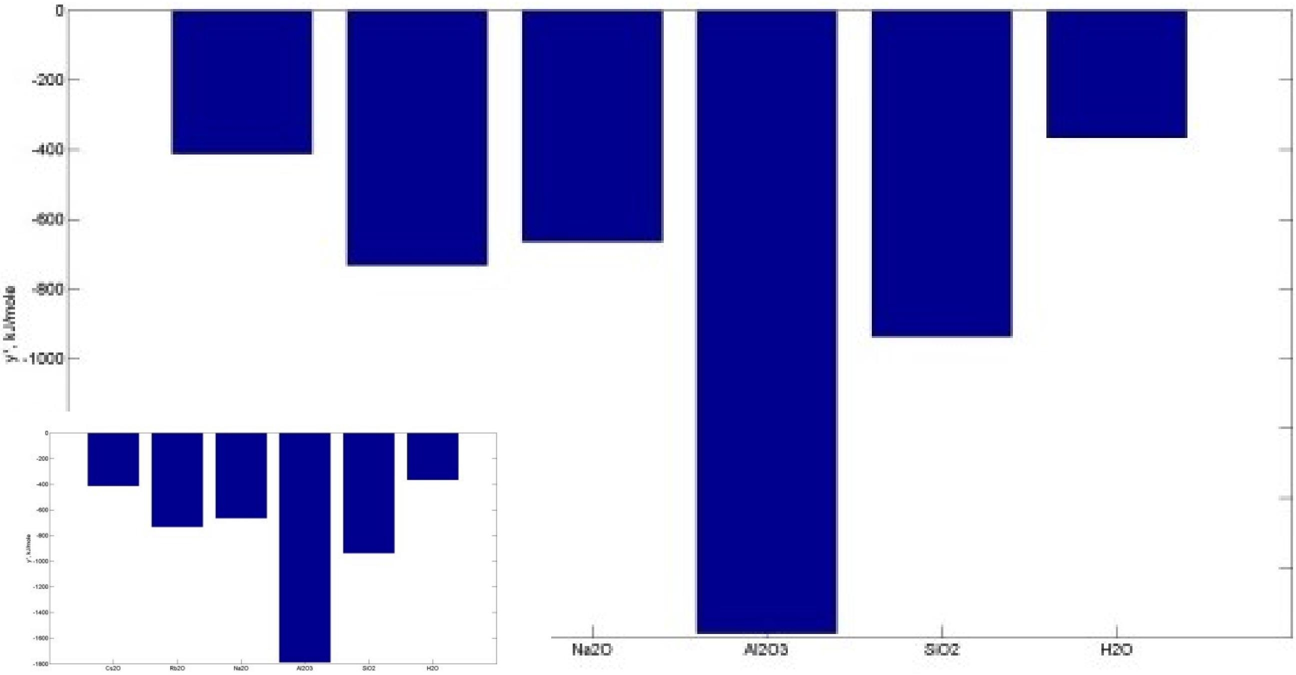

Fig. 1. The bar diagramm of oxides increments for standard enthalpy of formation from the elements H=-3104 kJ/mole of pollucite $Cs_{0.77}Rb_{0.04}Na_{0.14}[Al_{0.91}Si_{2.08}O_6]\cdot 0.34H_2O$.

The work was supported by RFBR and Government of Zabaykalskiy kray (project № 14-05-98012 r_Siberia_a)

References:

1. Eremin O.V. Estimation of the Standard Thermodynamic Potentials of Framework Ca-Aluminosilicates by Linear Programming//Geochemistry International 52 (2014) 788-793.
2. Eremin O.V, Epova E.S., Rusal' O.S., Filenko R.A., Bychinskii V.A., Chudnenko K.V., Fomichev S.V., Krenev V.A. The Unified Method for Computing Thermodynamic Properties of Natural Zeolites Based on Their Crystallochemical Formulas//Russian Journal of Inorganic Chemistry, 2016, Vol. 61, No. 8, pp. 1003–1012
3. Brundu A., Cerri G. Thermal transformation of Cs-clinoptilolite to CsAlSi5O12//Microporous and Mesoporous Materials 208 (2015) 44-49
4. Ogorodova L.P., Melchakova L.V., Kiseleva I.A., Belitsky I.A. Thermochemical study of natural pollucite//Thermochimica Acta 403 (2003) 251-256.
5. Sun P, Deore S., Navrotsky A. Formation and dehydration enthalpy of ion exchanged zeolite beta//Microporous and Mesoporous Materials 91 (2006) 15–22
6. Vipin A.K Ling S., Fugetsu B. Removal of Cs+ and Sr2+ from water using MWCNT reinforced Zeolite-A beads//Microporous and Mesoporous Materials 224 (2016) 84-88
7. Wu L., Navrotsky A., Lee Y, Lee Y. Thermodynamic study of alkali and alkaline-earth cation-exchanged natrolites//Microporous and Mesoporous Materials 167 (2013) 221–227

Eremin O.V.1), Borzenko S.A.1), Epova E.S.1), Rusal O.S.1), Bychinskii V.A.2) Estimation of the Gibbs free energy for fluorocarbonates of light lanthanides

1) Institute of natural resources, ecology and cryollogy SB RAS, Chita.

2) Institute of geochemistry SB RAS, Irkutsk. (yeroleg@yandex.ru)

Abstract. Based on experimental data (Gysi and Williams-Jones, 2015) the linear decomposition of the standard Gibbs energies of minerals bastnasite ($Ce_{0.5}La_{0.25}Nd_{0.2}Pr_{0.05}CO_3F$) and parisite ($CaCe_{0.95}La_{0.6}Nd_{0.35}Pr_{0.1}(CO_3)_3F_2$) have been obtained which can be used for calculations of free energies of these classes substances.

Keywords: Gibbs free energy, bastnesite, parisite.

Bastnasite - $(Ce,La,Y)CO_3F$ – is the main ore mineral of light lanthanides. In work (Gysi and Williams-Jones, 2015) the standard thermodynamic properties of bastnasite - $Ce_{0,5}La_{0,25}Nd_{0,2}Pr_{0,05}CO_3F$(Bast) and parisite - $CaCe_{0,95}La_{0,6}Nd_{0,35}Pr_{0,1}(CO_3)_3F_2$(Pari) have been determined. On the base of these data for reactions:

$$0.083Ce_2O_3+0.125La_2O_3+0.1Nd_2O_3+0.025Pr_2O_3+$$
$$+CO_2+0.333CeF_3=$$
$$=Ce_{0.5}La_{0.25}Nd_{0.2}Pr_{0.05}CO_3F \text{ (Bast)} \qquad (1)$$

$$CaO+0.142Ce_2O_3+0.3La_2O_3+0.175Nd_2O_3+$$
$$+0.05Pr_2O_3+3CO_2+0.667CeF_3=$$
$$=CaCe_{0.95}La_{0.6}Nd_{0.35}Pr_{0.1}(CO_3)_3F_2\text{(Pari)} \qquad (2)$$

the linear programming problems:

$$\min Gx,\ Ax=b,\ x\geq 0 \qquad (3)$$

have been formulated and solved, where G – standard Gibbs energies of formation from the elements for components of reactions (1,2) (1,2), x – their mole quantities, A – stoichiometric matrix, $Ax=b$, $x\geq 0$ – the conditions of mass balance in a closed system. Solutions y* of problems dual to (3):

$$y^*=\max by,\ A'y\leq G \qquad (4)$$

where ′ – transposing index, may be presented as linear decomposition of Gibbs energies of minerals – products of reactions (1,2) on stoichiometric increments of reagents (Eremin et al., 2015; Eremin, 2014):

$$G=\sum k_i y^*_I \qquad (5)$$

where k_i - stoichiometric coefficients and y* - potential of increments i.

Results of calculations are presented in table 1 and figures 1,2.

The calculated y* values can be used for estimations of the Gibbs free energies for fluorocarbonates of light lanthanides.

Table 1. The values of standard Gibbs energies used in calculations

Compounds	-G, kJ/mole	Calculated y* (1)	 y* (2)
Bastnasite $Ce_{0.5}La_{0.25}Nd_{0.2}Pr_{0.05}CO_3F$	1709.700 [Gysi and Williams-Jones, 2015]	1709.700	1724.597
Parisite $CaCe_{0.95}La_{0.6}Nd_{0.35}Pr_{0.1}(CO_3)_3F_2$	4571.500 [Gysi and Williams-Jones, 2015]	-	4571.500
Ce_2O_3	1706.202 [Yokokawa, 1988]	2075.451	2040.625
La_2O_3	1705.980 [Navrotsky et al., 2015]	2020.131	1953.243
Nd_2O_3	1720.649 [Navrotsky et al., 2015]	2068.462	2033.130
Pr_2O_3	1721.041 [Navrotsky et al., 2015]	2207.257	2157.931
CeF_3	1700.411 [Yokokawa,1988]	1863.312	1867.325
CO_2	394.384 [Reid et al., 1977]	401.097	430.685
CaO	604.048 [Yokokawa, 1988]	-	695.802

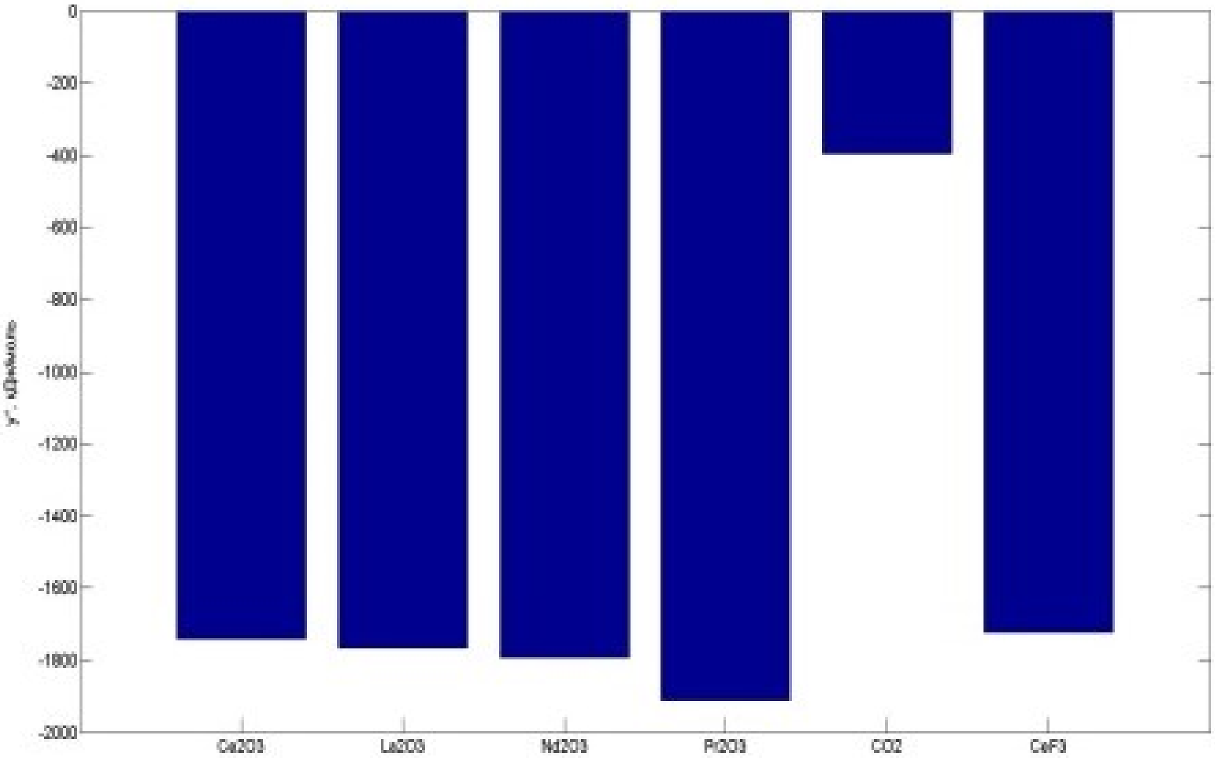

Fig. 1. The bar diagramm of y*(1) for bastnasite.

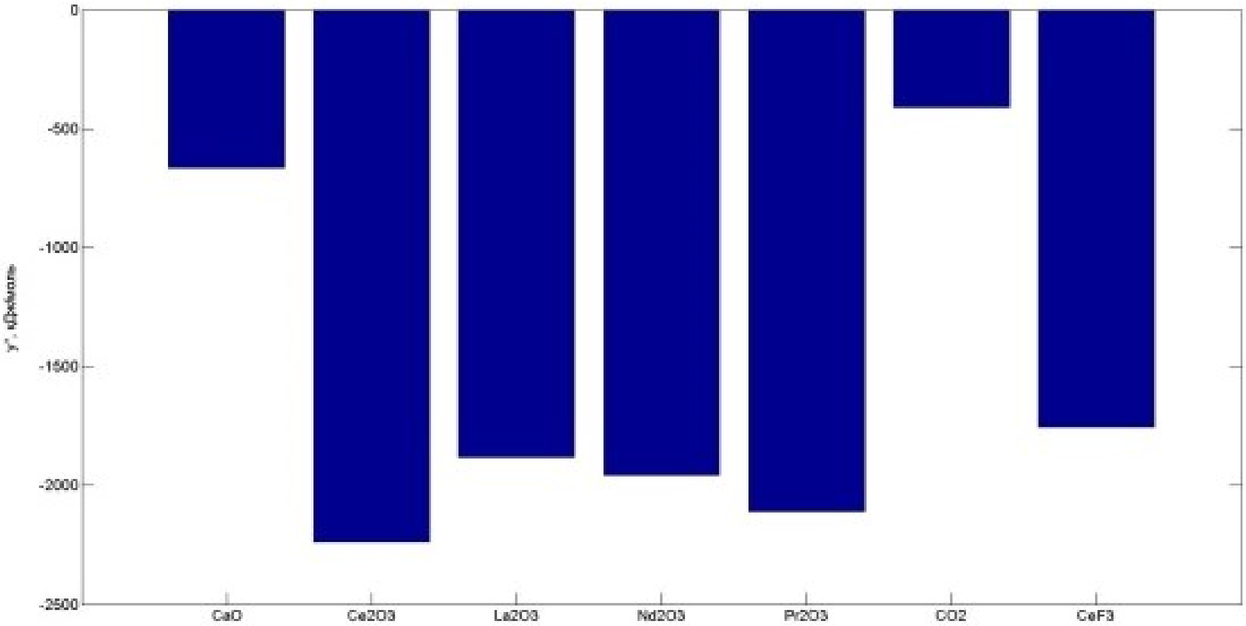

Fig. 2. The bar diagramm of y*(2) for parisite.

The work was supported by RFBR and Government of Zabaykalskiy kray (project № 14-05-98012 r_Siberia_a)

References:

1. Eremin O.V. Estimation of the Standard Thermodynamic Potentials of Framework Ca-Aluminosilicates by Linear Programming//Geochemistry International 52 (2014) 788-793.
2. Eremin O.V, Rusal' O.S., Bychinskii V.A., Chudnenko K.V., Fomichev S.V., Krenev V.A. Calculation of the Standard Thermodynamic Potentials of Aluminum Sulfates and Basic Aluminum Sulfates// Russian Journal of Inorganic Chemistry, 2015, Vol. 60, No. 8, pp. 950–957.
3. Gysi A.P., Williams-Jones A.E. The thermodynamic properties of bastnasite-(Ce) and parisite-(Ce)// Chemical Geology 392 (2015) 87-101.
4. Navrotsky A., Lee W., Mielewczyk-Gryn A., Ushakov S.V., Anderko A., Wu H., Riman R.E. Thermodynamics of solid phases containing rare earth oxides//J. Chem. Thermodynamics 86 (2015) 126-141.
5. Reid R., Prausnitz J., and Sherwood T. (1977), The

properties of gases and liquids, 3d edition, McGrawHill Book Company, New York, 592p.

6. Yokokawa H. (1988). Tables of thermodynamic properties of inorganic compounds. Journal of the national chemical laboratory for industry,Tsukuba Ibaraki 305, Japan, v.83, 27-118.

Sokolova T.S., Danilov B.S. Additive approach to estimating of standard thermodynamic functions of charoite

Institute of the Earth's Crust, Siberian Branch of the Russian Academy of Sciences
sokolovats@crust.irk.ru

Abstract. The values of standard thermodynamic functions, enthalpy of formation and entropy (ΔH^0_{298} и S^0_{298}), are required data for thermodynamic analysis of charoite formation. The experimental studies of enthalpy and entropy in some cases is very difficult and time laborious issue, therefore it is needed to use alternative calculation methods. The main idea of this work is to calculate of standard values of enthalpy and entropy of charoite, which is one of minerals alkaline calcium silicate group. Analysis of chemical compositions of charoite in studies (Rogova et al., 1978; Kraeff et al., 1980; Nikishova et al., 1985; Konev et. al., 1996; Matesanz et al., 2008; Correcher et al., 2008; Wang et al., 2014; etc.) is allowed us to determine a range of Ca, Na, K, Ba and Si oxides as constant. The chemical compositions were recalculated to 120 (121±2) cations, according to general charoite chemical composition (Rozhdestvenskaya et al., 2011). The additive approach to calculating of standard enthalpy and entropy of silicates from oxides (Kutolin, 1964; Babushkin et al., 1972; Maltsev et al., 2012) is gave the following results $\Delta H^0_{298} = -89550.8\pm1065.8$ $kJmol^{-1}$ and $\Delta S^0_{298} = 5751.2\pm62.7$ $Jmol^{-1}K^{-1}$. Thus, we first estimated the values of standard thermodynamic functions of charoite, what can contribute in solving the problem of charoite genesis conditions in the future.

The work was supported by the Russian Foundations of Basic Research (project No 14-45-04108).

Zakirov I.V., Suvorova V.A. The first experimental data on solubility of tin in the steam phase in the H_2O-SnO_2 system.

IEM RAS, Chernogolovka lera@iem.ac.ru

Abstract. Temperature dependence of tin content in a saturated steam phase of the H_2O-SnO_2 system is presented at 330-360C and pressure of saturated steam.

Keywords: content of tin, temperature dependence

Tin is a component of many hydrothermal systems. Depending on conditions it can is in II and IV valence state. In natural waters tin is present mainly at a type of gidroksokompleks, and in the HCl-containing waters ions of chlorine [1] can act as ligands. Sn shows amphoteric properties and in the wide range of pH neutral complexes – $Sn(OH)_2$ and $Sn(OH)_4$[2,3] dominate.

The behavior of Sn (II) in hydrothermal systems is studied quite well [3,4]. The behavior of Sn (IV) is studied poorly that his presence at solutions is controlled by low solubility of cassiterite (SnO_2) [4].

Solubility of Sn (IV) in a steam phase was studied on the original installation allowing to make sampling of in situ [5].

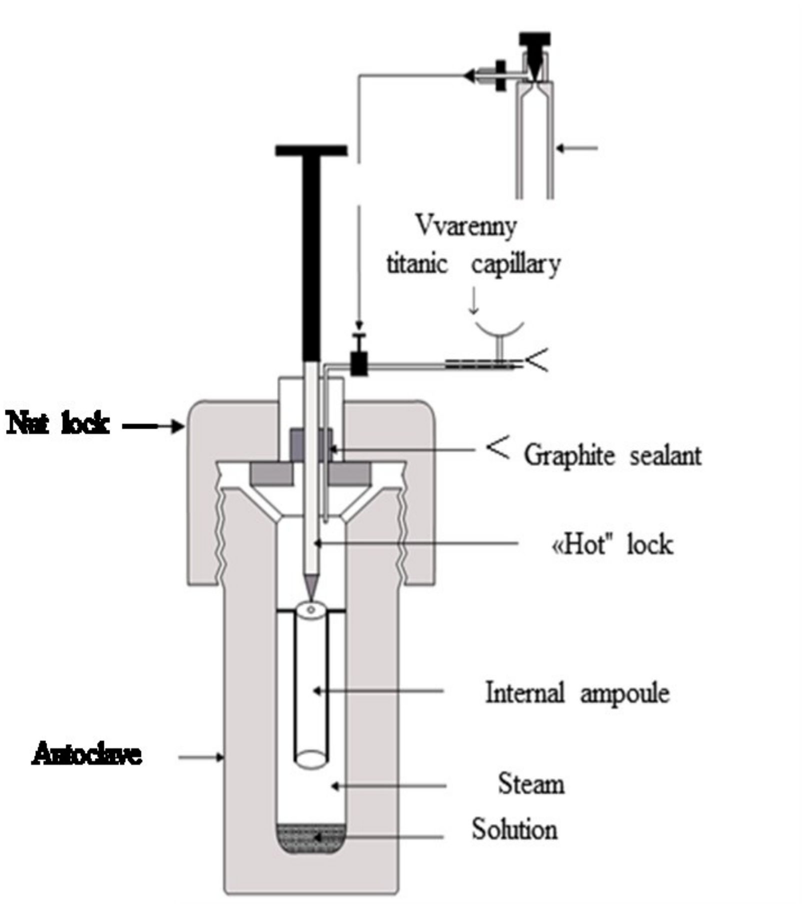

Fig. 1 Scheme of installation for selection of test of a gas phase experience

Condensate of steam was diluted 3%HNO_3 and analyzed by the ICP MS method. Results are presented in the table:

№	T° C	Sn, ppb
18	330	1376
19	330	1648
21	350	4784
22	350	4008
23	350	3810
24	360	5001
25	360	5865
26	360	5906

and in the drawing, where points – an average from several experiences.

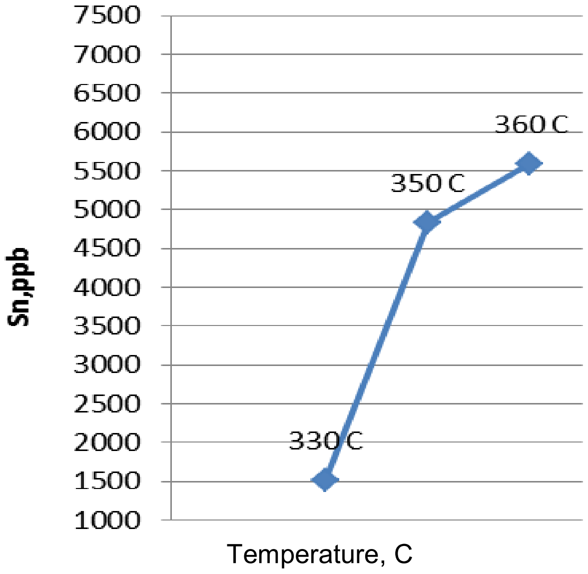

Authors express gratitude of Ya. V. Bychkova for carrying out ICP MS of the analysis, and also A. V. Zotova for valuable remarks on the equipment and a technique of carrying out an experiment.

Work is performed with financial support of RNF (grant No. 14-17-00366).

References:

1. Sorokin VI, Dadze TP (1994) Solubility and complex formation in the systems Hg-H_2O, S-H_2O, SiO_2-H_2O and SnO_2-H_2O. In: Fluids in the Crust. Springer Netherlands, Dordrecht, pp 57–93
2. Séby F, Potin-Gautier M, Giffaut E, et al (2001) A critical review of thermodynamic data for selenium species at 25°C. Chem Geol 171:173–194. doi: 10.1016/S0009-2541(00)00246-1
3. Cigala RM, Crea F, De Stefano C, et al (2012) The inorganic speciation of tin(II) in aqueous solution. Geochim Cosmochim Acta 87:1–20. doi: 10.1016/j.gca.2012.03.029
4. Migdisov AA, Williams-Jones AE (2005) An experimental study of cassiterite solubility in HCl-bearing water vapour at temperatures up to 350 °C. Implications for tin ore formation. Chem Geol 217:29–40. doi: 10.1016/j.chemgeo.2004.11.018
5. Zakirov IV, Sretenskaya NG Methods of experimental determination of the composition of the phases in the heterogeneous conditions // Experimental problems of geology. M .: Publishing House of Science. 1994. pp 664-667

Shornikov S. I. Thermodynamic properties of the CaO–MgO–SiO_2 melts

Vernadsky Institute of Geochemistry and Analytical Chemistry of RAS, Moscow

Abstract. Within the framework of the developed semi-empirical model, the calculations were made of thermodynamic properties of the CaO–MgO–SiO_2 melts in the temperature region 1600–2400 K. The calculated values of the oxide activities and the mixing energies of melts are compared with available experimental information.

Key words: thermodynamic properties of oxide melts, the CaO–MgO–SiO_2 system

Physico-chemical properties of the compounds of the CaO–MgO–SiO_2 system and their melts are of great interest to the geochemistry. In particular, several compounds of this system (forsterite, diopside and akermanite) are part of the Ca–Al–Inclusions (CAIs) in chondrites.

This investigation presents the calculation of thermodynamic properties of the CaO–MgO–SiO_2 melts at temperatures from 1600 to 2400 K within framework of the ideal associated solutions theory. The aim of the present study was to clarify the parameters used by semi-empirical model for calculation of oxide activities in the CaO–MgO–FeO–Al_2O_3–TiO_2–SiO_2 multicomponent melts in a wide range of compositions and temperatures. The model parameters, as earlier [Shornikov, 2008] were calculated from the experimental and theoretical data [Glushko et al., 1978–1982; Bale et al., 2009; Shornikov and Yakovlev, 2015].

The initial thermodynamic data considered 21 condensed phases (13 solid and 8 liquid) and 17 gas species, these components are listed in the Table 1. The same table 1 gives the calculated values of the Gibbs formation energies from elements ($\Delta_f G°_T$) for the compounds and the vapor species over the CaO–MgO–SiO_2 system. They were used for the calculation of the equilibrium conditions in the system at a given composition and temperature. The required equation solution for the total Gibbs energy for the system studied was found by the widely used approach, namely the Gibbs energy minimization method.

The calculated values of the oxide activities (a_i) in the CaO–MgO–SiO$_2$ melts obtained in the present study (Fig. 1) are coincide approximately to the same results, which are the most widely cited in the literature [Rein and Chipman, 1965]. The observed differences are due to the indirect definition of the CaO and MgO activities by Rein and Chipman, used the Schuhmann's metod [Schuhmann, 1955]. It evidenced by the course of the concentration dependences of the mixing energy in melts (ΔG^m) under consideration (Fig. 2). As can be seen from Fig. 2, the mixing energy in melts, obtained by Rein and Chipman, are not indicative of the minimum, corresponding to the diopside CaMgSiO$_4$, and differ from the calculated values coincide with data obtained by the Knudsen mass-spectrometric effusion method [Shornikov et al., 1997] by on 4 kJ/mole approximately.

Table 1. The Gibbs energy of formation from elements of condensed phases and vapor species over the CaO–MgO–SiO$_2$ system at 2000 K, calculated in present study

Condensed phases				Gas phase	
Solid phases	$\Delta_f G°_{2000}$, kJ/mole	Liquid phases	$\Delta_f G°_{2000}$, kJ/mole	Vapor species	$\Delta_f G°_{2000}$, kJ/mole
CaO	–421.511	CaO	–409.450	Ca	–21.080
$CaSiO_3$	–1058.628	$CaSiO_3$	–1064.401	Ca_2	77.075
Ca_2SiO_4	–1531.242	Ca_2SiO_4	–1522.120	CaO	–74.308
Ca_3SiO_5	–1945.934			Mg	–57.263
$Ca_3Si_2O_7$	–2577.486			Mg_2	34.314
MgO	–376.430	MgO	–345.380	MgO	–108.759
$MgSiO_3$	–956.936			Si	167.228
Mg_2SiO_4	–1360.399	Mg_2SiO_4	–1351.811	Si_2	216.304
$CaMgSiO_4$	–1461.894			Si_3	265.892
$CaMgSi_2O_6$	–2038.188	$CaMgSi_2O_6$	–2065.893	Si_4	409.396
$Ca_2MgSi_2O_7$	–2478.460	$Ca_2MgSi_2O_7$	–2498.156	SiO	–248.438
$Ca_3MgSi_2O_8$	–2976.156			SiO_2	–314.875
SiO_2	–550.476	SiO_2	–550.520	Si_2O_2	–546.135
				O	121.662
				O_2	0.000
				O_3	273.851
				O_4	193.351

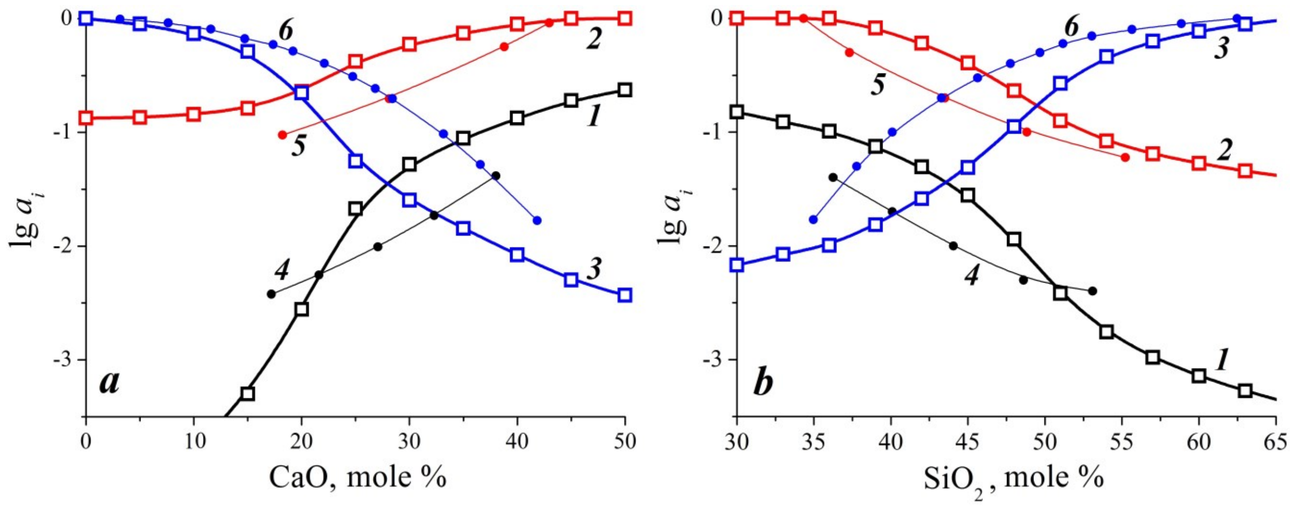

Fig. 1. The activity of CaO (*1*, *4*), MgO (*2*, *5*) and SiO$_2$ (*3*, *6*) in the 2MgO·3SiO$_2$–CaO melts (*a*) and in the CaO·MgO–SiO$_2$ melts (*b*) at 1873 K: *1–3* – obtained in the present study and *4–6* – [Rein and Chipman, 1965].

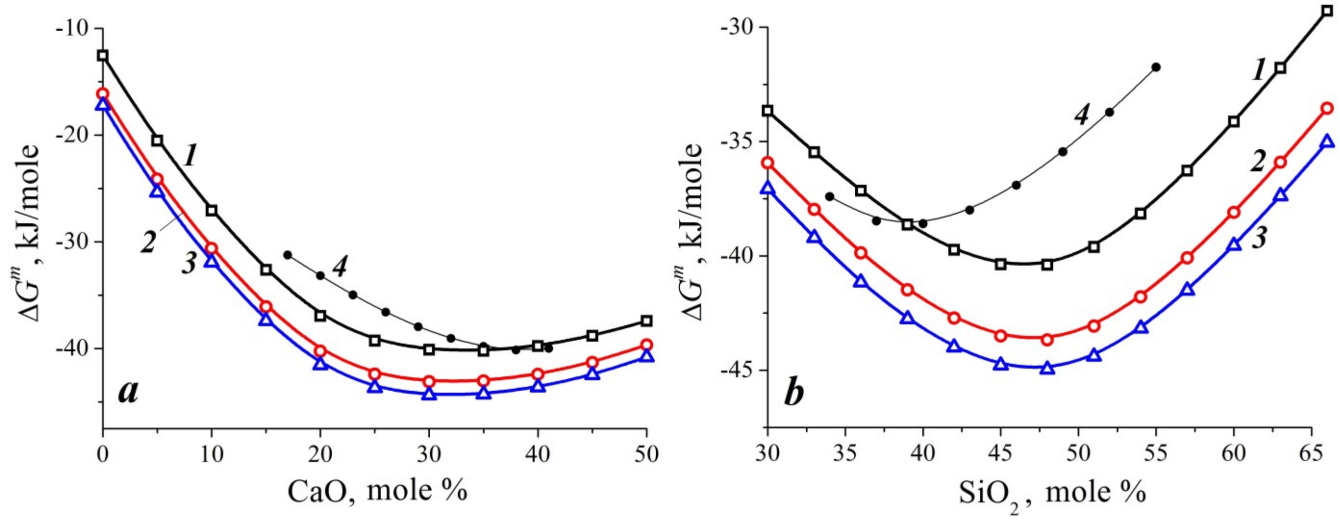

Fig. 2. The mixing energy in the $2MgO \cdot 3SiO_2$–CaO melts (*a*) and in the $CaO \cdot MgO$–SiO_2 melts (*b*) at 1873 (*1*, *4*), 1973 (*2*) and 2073 K (*3*): *1–3* – obtained in the present study and *4* – [Rein and Chipman, 1965].

The present study was supported by RAS Presidium's Program #7 (Experimental and theoretical studies of Solar system objects and star planetary systems. Transients in astrophysics).

References:

1. Bale, C. W., E. Belisle, P. Chartrand, S. A. Degterov, G. Eriksson, K. Hack, I.-H. Jung, Y.-B. Kanga, J. Melancon, A. D. Pelton, C. Robelin, S. Petersen (2009). FactSage thermochemical software and databases – recent developments. *CALPHAD*, vol. 33, no. 2, pp. 295–311.
2. Glushko, V. P., L. V. Gurvich, G. A. Bergman, I. V. Veitz, V. A. Medvedev, G. A. Khachkuruzov, V. S. Youngman (1978–1982). Thermodynamic properties of individual substances. M.: Nauka.
3. Rein, R. H. and J. Chipman (1965). Activities in the liquid solution SiO_2–CaO–MgO–Al_2O_3 at 1600 °C. *Trans. Met. Soc. AIME*, vol. 233, no. 2, pp. 415–425.
4. Schuhmann, R. (1955). Application of Gibbs-Duhem equations to ternary systems. *Acta Met.*, vol. 3, no 3, pp. 219–226.
5. Shornikov, S. I., V. L. Stolyarova, M. M. Shultz (1997). Vaporization and the thermodynamic properties of diopside. *Russ. J. Phys. Chem.*, vol. 71, no. 2, pp. 174–178.
6. Shornikov, S. I. (2008). Thermodynamic properties of the MgO–Al_2O_3–SiO_2 melts. *Experiment in Geosciences*, vol. 15, no. 1, pp. 147–149.
7. Shornikov, S. I. and O. I. Yakovlev (2015). High-temperature thermodynamic properties of CAI minerals. *XXXXVI Lunar. Planet. Sci. Conf.*, Abs. #1270

Shornikov S.I. High-temperature thermodynamic properties of $MgAl_2O_4$ spinel

Vernadsky Institute of Geochemistry and Analytical Chemistry of RAS, Moscow

Abstract. A mass spectrometric Knudsen effusion method was used to investigate the $MgAl_2O_4$ spinel evaporation at 1850–2300 K. The oxide typical molecular ions as well as the MgAlO ion were identified in the gas phase over spinel. The oxide activities and the Gibbs energy of spinel formation from oxides were obtained. The enthalpy and entropy of spinel formation from oxides, equal to –12.02±1.14 kJ/mole and 5.03±0.56 J/(mole·K), correspondingly, and the enthalpy of melting equal to 55.81±4.62 kJ/mole are corresponding to literature information.

Key words: mass spectrometric Knudsen effusion method, thermodynamics of evaporation, spinel

The $MgAl_2O_4$ spinel is of particular interest to cosmochemistry as a basic mineral (up to 24 vol. %) of all types of substances of the refractory Ca–Al–Inclusions (CAIs). They are the earliest objects in the Solar system with an unusual isotopic characteristics and founded in carbonaceous chondrites. Spinel is also a dominant mineral in the Wark-Lowering rims (up to 71 vol. %), which are formed in the flesh-heating process (above the temperature of 2300 K) due to changes in the CAIs mineral composition, which caused by the enrichment of refractory minerals (mainly spinel and perovskite and pyroxene) due to melilite [Wark and Boynton, 2001].

That's why, the thermodynamic data characterized the evaporation processes of spinel at temperatures exceeding 1500 K acquired a special interest. The thermochemical information is based on measurements of the specific heat of the spinel, their differences are exceeded 10 J/(mole·K), leading to systematic deviations. Studies of the heterogeneous equilibria in oxide melts including spinel [Kalyanram and Bell, 1961; Rein and Chipman, 1965; Chamberlin et al., 1995; Fujii et al., 2000] are inaccurate, the differences in the Gibbs energy values exceed 15 kJ/mole (on 1 mole of the compounds), the values of enthalpy and entropy of spinel formation has a considerable error. Thermochemical data on the value of the enthalpy of spinel melting are contradictory. The information on the evaporation processes of spinel are scarce [Rutman et al, 1969; Sasamoto et al., 1981] and it limited the values of partial vapor pressure of the gas phase dominant component (atomic of magnesium).

In the present study we have investigated the evaporation of a stoichiometric spinel from Knudsen effusion molybdenum cells, the gas phase composition over spinel was identified by mass spectrometric method in the temperature range 1850–2300 K. The ions, characteristic to the oxides of magnesium and aluminum, as well as the MgAlO complex gaseous oxide ion were detected in the mass spectra of vapor over spinel.

The established molecular composition of the gas phase over spinel allowed to make the assumption that the spinel evaporation occurs mainly by heterogeneous reactions, typical for the individual oxide's vaporization. The MgAlO molecular form presented in minor amounts in the gas phase over spinel and indicated about the possible heterogeneous reaction:

$$[MgAl_2O_4] = (MgAlO) + (Al) + 3(O). \qquad (1)$$

The partial pressures values of the vapor species over spinel (p_i) in the temperature range 1850–2090 K were determined by the Hertz-Knudsen equation and shown in the Fig. 1. There was a noticeable change of spinel composition at higher temperatures due to the preferential evaporation of the vapor species, belonging to the magnesium oxide.

The activity values of oxides in spinel were calculated by the Lewis equation:

$$a_i = p_i / p_i^\circ \qquad (2)$$

(p_i and p_i° – the partial pressures values of the vapor species over spinel and simple oxide, respectively). The activity values of oxides in spinel in the crystalline state at higher temperatures (2050–2300 K) were found using the data [Shornikov and Archakov, 2001] on the $MgAl_2O_4$–SiO_2 melts evaporation. The value of the Gibbs energy of spinel formation $\Delta G_T(MgAl_2O_4)$ was found by the relation:

$$\Delta G_T(MgAl_2O_4) = RT\sum x_i \ln a_i\ , \qquad (3)$$

where x_i is the mole fraction of oxide ($\sum x_i = 1$). The values of enthalpy $\Delta H_T(MgAl_2O_4)$ and entropy $\Delta S_T(MgAl_2O_4)$ of spinel formation has been calculated using by the least squares method from the $\Delta G_T(MgAl_2O_4)$ temperature dependences in the approximation of constancy of these values in the considered temperature interval and equal to –12.02±1.14 kJ/mole and 5.03±0.56 J/(mole·K), respectively, and are consistent with available data.

Thermodynamic information on the oxide activities in the $MgAl_2O_4$–SiO_2 melts [Shornikov and Archakov, 2001] allowed also to calculate the Gibbs energy values of spinel in the liquid state and find of enthalpy and entropy of spinel formation, equal to 43.79±4.84 kJ/mole and 28.09±1.64 J/(mole·K), respectively, and calculate the enthalpy of spinel melting, equal to 55.81±4.62 kJ/mole at the temperature of 2420±25 K.

The values of $\Delta H_T(MgAl_2O_4)$ and $\Delta S_T(MgAl_2O_4)$ determined in the present study are correlated with results of the Knudsen mass spectrometric effusion method [Rutman et al, 1969; Sasamoto et al., 1981], performed at lower temperatures. Information obtained in studies of heterogeneous equilibria involving spinel [Kalyanram and Bell, 1961; Rein and Chipman, 1965; Chamberlin et al., 1995; Fujii et al., 2000] does not contradict the results of the present study, however they have a significant error. The values characterizing the spinel melting found in the present work are in good agreement with the experimental data, obtained by Richet [Richet, 1993].

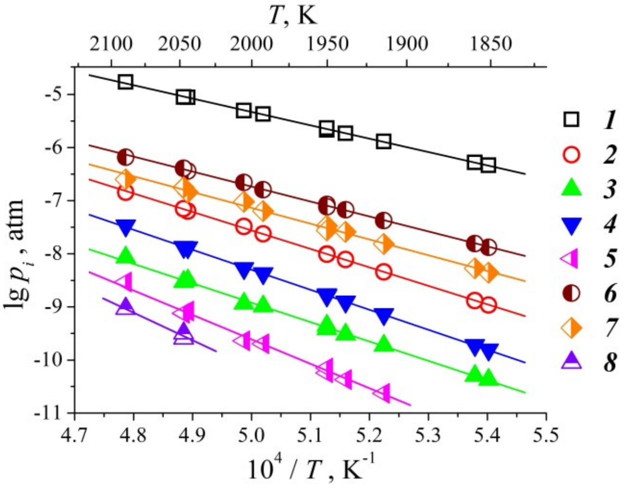

Fig. 1. The partial pressures of vapor species over spinel: *1* – Mg, *2* – MgO, *3* – Al, *4* – AlO, *5* – Al_2O, *6* – O, *7* – O_2 and *8* – MgAlO.

Thus, the spinel evaporation from the molybdenum cell was studied by the Knudsen mass spectrometric effusion method studied at 1850–2300 K. The molecular components typical for simple oxides forming the spinel and also in a small number of the MgAlO complex gaseous oxide were identified in the gas phase over spinel. The partial pressures values of vapor species over spinel were determined at the first time. The spinel thermodynamic data related to their crystalline and liquid state were determined too.*

The present study was supported by RAS Presidium's Program #7 (Experimental and theoretical studies of Solar system objects and star planetary systems. Transients in astrophysics).

References:

1. Chamberlin, L., J. R. Beckett, E. Stolper (1995). Palladium oxide equilibration and the thermodynamic properties of $MgAl_2O_4$ spinel. *Amer. Miner.*, vol. 80, no. 3–4, pp. 285–296.
2. Fujii, K., T. Nagasaka, M. Hino (2000). Activities of the constituents in spinel solid solution and free energies of formation of MgO, $MgO{\cdot}Al_2O_3$. *JISJ Int.*, vol. 40, no. 11, pp. 1059–1066.
3. Kalyanram, M. R. and H. B. Bell (1961). Activities in the system $CaO–MgO–Al_2O_3$. *Trans. Brit. Ceram. Soc.*, vol. 60, no. 2, pp. 135–145.
4. Rein, R. H. and J. Chipman (1965). Activities in the liquid solution $SiO_2–CaO–MgO–Al_2O_3$ at 1600 °C. *Trans. Met. Soc. AIME*, vol. 233, no. 2, pp. 415–425.
5. Richet, P. (1993). Melting of forsterite and spinel with implications for the glass transition of Mg_2SiO_4 liquid. *Geophys. Res. Lett.*, vol. 20, no. 16, pp. 1675–1678.
6. Rutman, D. S., I. L. Schetnikova, T. S. Ignatova, E. I. Kelareva, L. V. Uzberg, G. A. Semenov (1969). The study of the evaporation process of refractory materials based on MgO and ZrO_2. *Trudy Vostochnogo instituta ogneuporov,* no. 9, pp. 143–161 [in Russian].
7. Sasamoto, T., H. Hara, T. Sata (1981). Mass spectrometric study of the vaporization of magnesium oxide from magnesium aluminate spinel. *Bull. Chem. Soc. Japan*, vol. 54, no. 11, pp. 3327–3333.
8. Shornikov, S. I. and I. Yu. Archakov (2001). High temperature mass spectrometric study of vaporization processes and thermodynamic properties in the $MgAl_2O_4–SiO_2$ system. *High Temperature Corrosion and Materials Chemistry III*, vol. 2001–12, pp. 322–329.
9. Wark, D., and W. V. Boynton (2001). The formation of rims on calcium-aluminum-rich inclusions: Step I – Flash heating. Met. Planet. Sci., vol. 36, no. 8, p. 1135–1166.

Mironenko M.V., Cherkasova E.V. Thermodynamic modeling behavior of bromide in processes of evaporation and freezing of sea water.

V.I. Vernadsky Institute RAS, (mironenko@geokhi.ru)

Abstract. The work is an extension of FRZCHEM model [Marion et al., 2010]. Entering Br^- into sodium, potassium, calcium, and magnesium chlorides has been described in terms of ideal binary solid solutions "chloride-bromide". Activity products of pure bromides, as functions of temperature, were calculated from reference experimental data on their solubilities and from values of water activities and ion activity coefficients at saturated concentrations for various temperatures. The last values were calculated using temperature-dependent Pitzer interaction parameters, estimated by Marion et al., 2009. The algorithm of calculating chemical equilibria was significantly modified. We modeled bromide behavior during fractional evaporation at 25 C and in process of fractional freezing of sea water.

Keywords: bromide, seawater, Pitzer equations, solid solutions, brines, chemical equilibria.

It is known that during evaporation of seawater a ratio Br^-/Cl^- increases in the remaining brine [Valiashko et al., 1966]. Under natural conditions bromine does not form own solids, but isomorphically replaces chlorine in chlorides. Distribution of bromine between a salt and aqueous solution usually is described in terms of empiric coefficients of fractionating. It has been experimentally shown [Siemann and Schramm, 2002; 2000] that at low aqueous Br^- contents (less than $5{\cdot}10^2$ μg/g) coefficients of fractionating among chlorides and solution increase as aqueous bromine concentration decreases, and they are approximately constant at higher concentrations. Bromine contents in seawater are much higher. This gives reasons to use a model of ideal solid solution for entering seawater bromide into solid chlorides.

We took activity products of chlorides from FREZCHEM database [Marion et al., 2010]. To calculate activity products of bromides at various temperatures we used data from reference books on solubility [Reference books on solubility of salt systems,1953; Reference books on solubility, 1961]: NaBr, $NaBr{\cdot}2H_2O$ (Seidell, 1940); KBr (Getman, 1935); $MgBr_2{\cdot}6H_2O$, $MgBr_2{\cdot}8H_2O$ (Getman, 1935); $CaBr_2{\cdot}6H_2O$ (Kremers, 1858; Rakowsky, Garrett, 1954; Etard, 1894). There are few data for Br-carnallite $KMgBr_3{\cdot}6H_2O$ for 25^0C only (Boekke, 1908; Nikolaev, 1935). Activity coefficients of Na^+, K^+, Mg^{2+}, Ca^{2+}, and Br^-, as well as water activities were calculated on the basis of Pitzer binary (plus ternary K-Mg-Br for Br-carnallite) interaction parameters, estimated in [Marion et al., 2009].

Calculated parameters of dependencies of activity products of bromides on temperature $\Delta G/RT=-ln(K)=a_0+a_1{\cdot}T+a_2{\cdot}T^2+a_3{\cdot}T^3+a_4/T+a_5{\cdot}ln(T)$ are shown in the table.

The obtained constants together with Pitzer interaction parameters from [Marion et al., 2009] make possible to reproduce adequately experimental diagrams of state of binary systems bromide-water, particularly $NaBr-H_2O$ (Fig.1).

Table. Parameters of temperature dependencies of activity products of bromides, calculated in this study

Salt	a_0	a_1	a_2	a_3	a_4	a_5
KBr	18280.60392	46.32501	-0.080388	6.26E-05	-44547.31116	-4643.10026
NaBr	18.82133	-0.058432	3.44E-06	5.66E-08	-3051.432	1.615122
$NaBr*2H_2O$	220530.535	242.10902	-0.283702	0.000165848	-3243466.366	-45810.8338
$CaBr_2*6H_2O$	38152.29528	51.07134	-0.0700075	4.76E-05	-490774.0595	-8209.25765
$MgBr_2*6H_2O$	-15376.23921	-22.218449	0.03038172	-0.00001998	170461.3439	3379.450597
$MgBr_2*8H_2O$	-1215.4775	14.9694	-0.0622	8.6549E-5	0	0
$KMgBr_3*6H_2O$	-6.22126	0	0	0	0	0

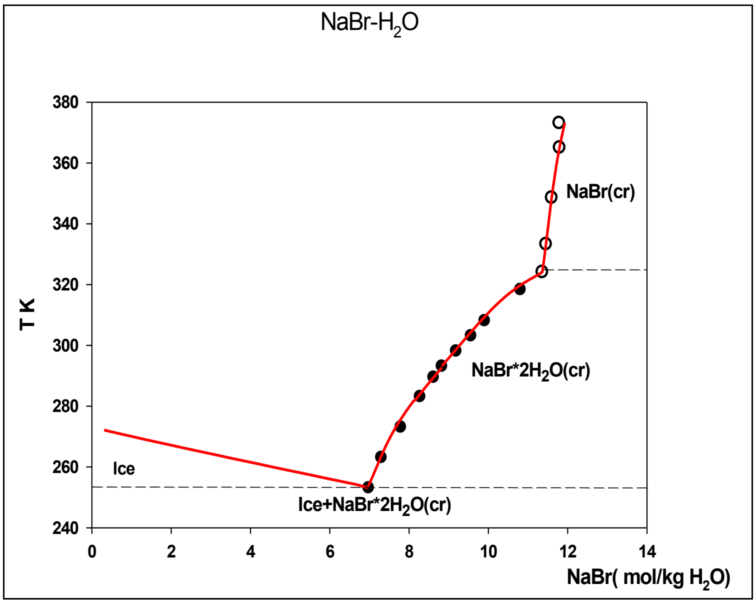

Fig. 1 Experimental (dots) and calculated (lines) diagram of state of the system $NaBr-H_2O$

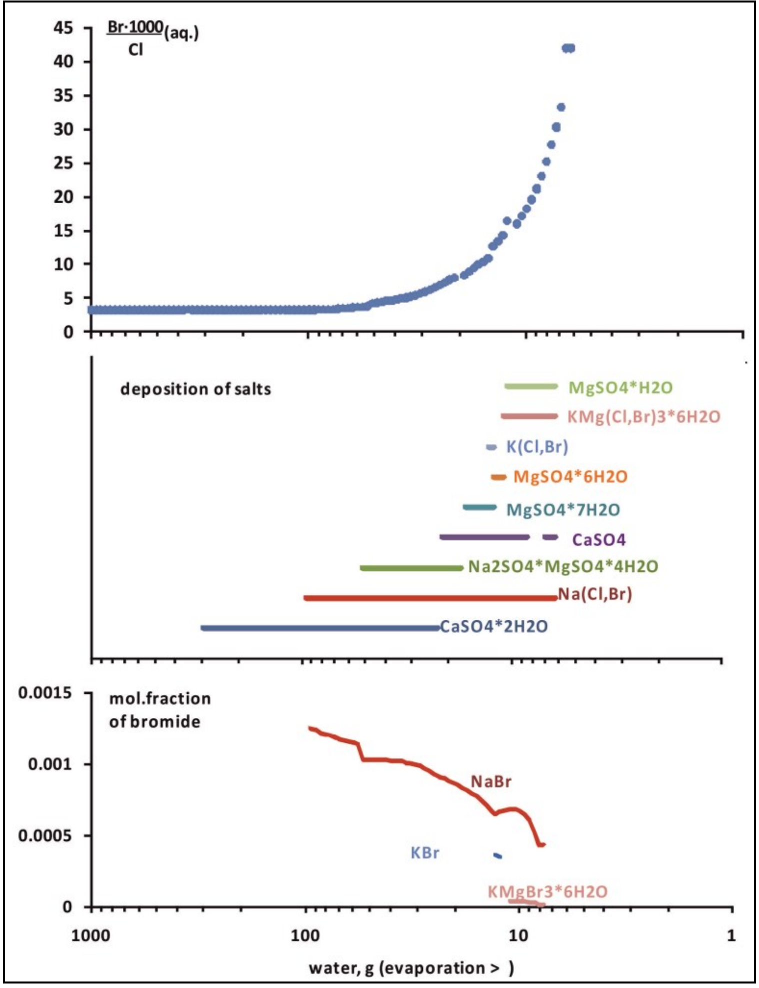

Fig. 2. Calculated behavior of bromine during fractional evaporation of model seawater at 25°C.

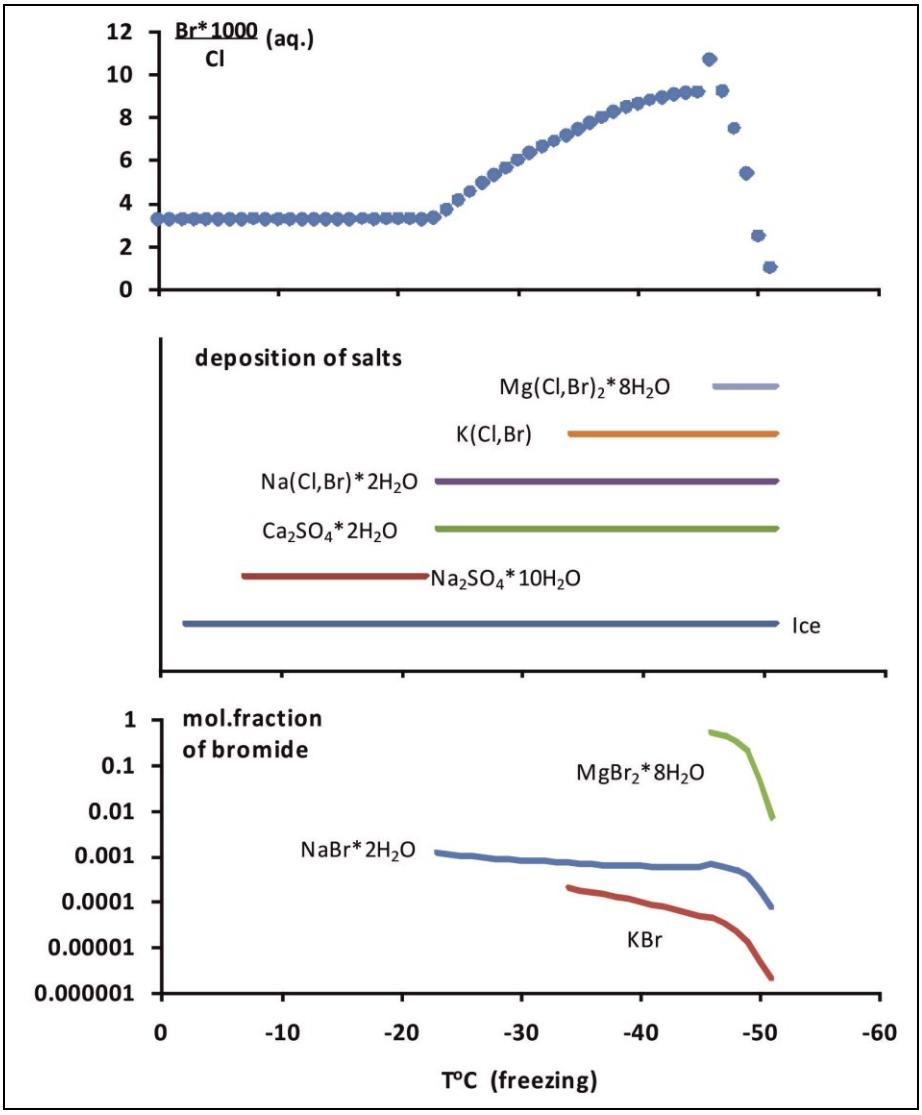

Fig. 3. Calculated behavior of bromine during model seawater freezing

We calculated bromine behavior during fractional seawater evaporation (Fig. 2) and seawater freezing (Fig. 3) in the H_2O-Na-K-Ca-Mg-Cl-SO_4-Br system. Temperature dependencies of Pitzer binary and ternary interaction parameters were taken from [Marion et al., 2009].

Thus we extended FREZCHEM model for bromine.

Acknowledgments. Authors thank V. B. Polyakov for his kind help in approximation of temperature dependencies of solubility constants. A study was partially supported by RFBR (grant 14-05-00128).

References:

1. Valiashko M.G., Zerebtsova I.K., Sadykov L.Z. 1966. Geochemical methods of prospecting deposits of potassium salts. Publishing house of Moscow university. 73 p. (*In Russian*)
2. Reference book on solubility of salt systems. V. 1. 1953. Goshimizdat. (*In Russian*)
3. Reference book on solubility. V. 1. 1961. Publishing house of Academy of Sciences of USSR. . (*In Russian*)
4. Marion G.M, Catling D.C., Kargel J.S. 2009. Br/Cl partitioning in chloride minerals in the Burns formation on Mars. Icarus. 200. 436–445.
5. Marion G.M., Mironenko M.V., Roberts M.W. 2010. FREZCHEM: A geochemical model for cold aqueous solutions. Computers and geosciences. 36.1.10-15.
6. Siemann M., Schramm M. 2000. Thermodynamic modelling of the Br partition between aqueous solutions and halite. Geochimica et Cosmochimica Acta. 64. 10. 1681–1693.
7. Siemann M.G., Schramm M. 2002. Henry's and non-Henry's law behavior of Br in simple marine systems. Geochimica et Cosmochimica Acta. 66. 8. 1387–1399.

UDC 548.55 Grazhdannikov S.A., Kurus' A.F., Krinitsyn P.G., Isaenko L.I., Drebushchak V.A. $LiGaTe_2$ crystal growth, modeling of the crystal growth process.

V.S. Sobolev Institute of Geology and Mineralogy SB RAS, Nikolaev Institute of Inorganic Chemistry SB RAS, Phys. Dep. NSU, Novosibirsk (sagwerbs@yandex.ru, pallasa55@rambler.ru, krinitsin_family@ngs.ru, lisa@igm.nsc.ru, dva@igm.nsc.ru)

Abstract. This paper presents recent data on $LiGaTe_2$ crystal growth. Specifically the latest DTA data of the synthesized charge and heat capacity anomalous temperature dependence are shown. The set of phases in addition to LGT, both at the sample heating and cooling steps, is observed. Also the newest 4-zone furnace construction based on the numerical modeling is presented.

Keywords: bulk crystal growth, nonlinear optics, Bridgman-Stockbarger technique, heat capacity, DTA, numerical modeling.

$LiGaTe_2$ (LGT) is a promising converter of laser radiation in the mid-IR range. The crystal has a wide transmission area (T = 0.52 - 21 μm), high nonlinear susceptibility (d36 = 43 pm/V) in combination with a high birefringence coefficient (Δn = 0.09) [Isaenko L. et al, 2003; Yelisseyev A. et al., 2015]. During the investigation we found the optimum charge composition for stoichiometric crystal growth and the charge's melting point was determined by DTA. Synthesized charge DTA data shown in Figure 1 indicate the primarily $LiGaTe_2$ ($T_{melting}$=945K) phase presence during the heating step. The cooling from the melt step occurs 945K peak, which corresponds to the $LiGaTe_2$ melting, and 739K peak corresponding to the melting point of the Te°, $LiTe_3$ and Ga_2Te_5 phases. We have also observed lithium carbide (Li_2C_2) phase with a melting point of 845K. The data confirm the Li_2Te excess over the stoichiometric composition choice validity.

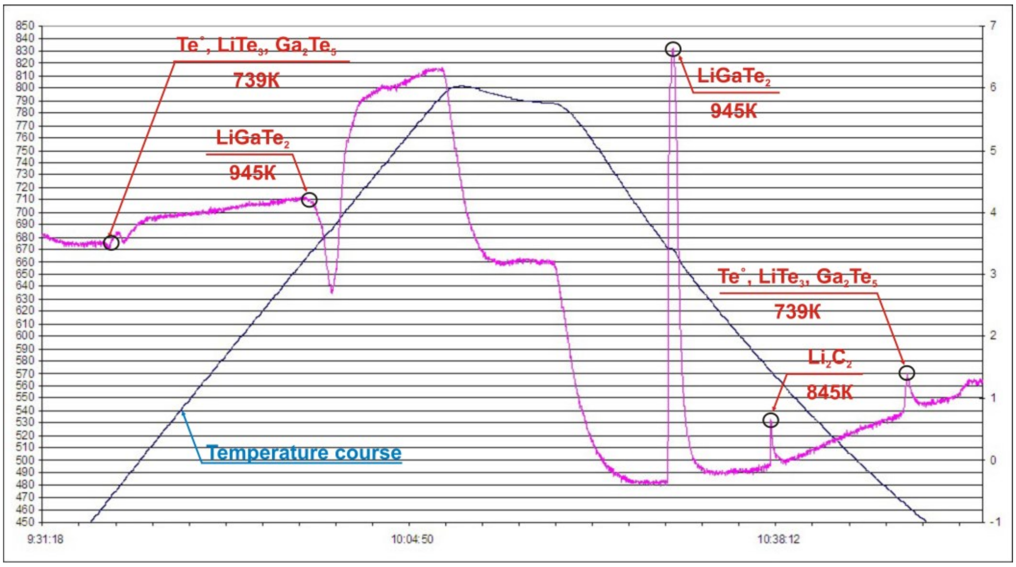

Fig. 1. Dependence of the energy absorbed and the surface temperature from the distance

LGT crystals up to 8 mm were obtained by the Bridgman-Stockbarger technique. We used the furnace with a controlled heat exchanger. The dependence of the heat capacity of the LGT crystal temperature (1) was examined.

$$C_p(T) = 100.01 + 0.0219 \cdot T - 191210 \cdot T^{-2} \qquad (1)$$

Heat capacity specific temperature variations are shown in Figure 2 and demonstrate the absence of phase transitions in this temperature range. The features are that all the experimental points and the curve, respectively, are located above the $3R$ per average gm-atom classical limit (for LGT it is 100 J/mol·K).

TGA data, shown in Figure 3, have presented no change in LGT sample weight up to 673 K.

It is known that for high-quality crystal growth it is important to provide either flat or convex crystallization front with respect to the growing crystal [Wilke K.Th., 1973]. The concave front increases the crystal doubling probability, as well as stimulates the generation of dislocations due to mechanical stresses occurring in the crystal. Thermoelastic stresses, which are the source of shear dislocations, occur during the crystal growth due to the non-constant inside temperature gradient [Indenbom V.L., 1957; Dash W.C., 1957]. Single crystal quality with a small plastic deformation zone amount is particularly influenced by thermal stress.

To optimize the LGT single crystal growth process STR Group Crystal Growth Simulation (CGSim) was applied. During the mathematical modeling process the thermal unit geometry has been designed, as well as the temperature profile configuration inside it has been selected. It is assumed that this will provide the single crystal growth by the slightly convex crystallization front with respect to the crystal as illustrated in Figure 4.

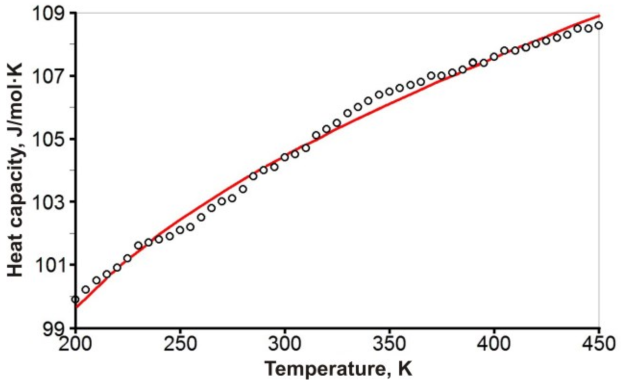

Fig. 2. LGT heat capacity of the temperature dependence.

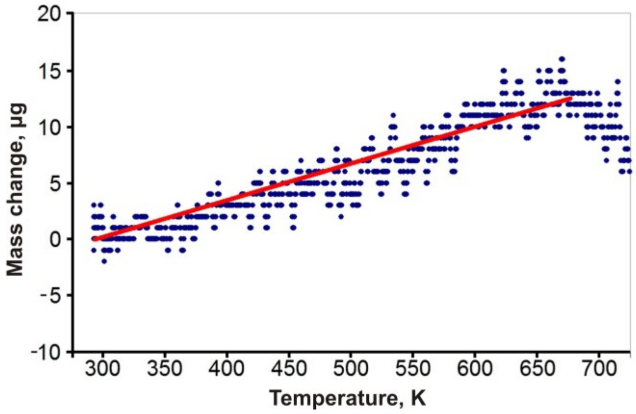

Fig. 3. LGT sample mass changing while heating.

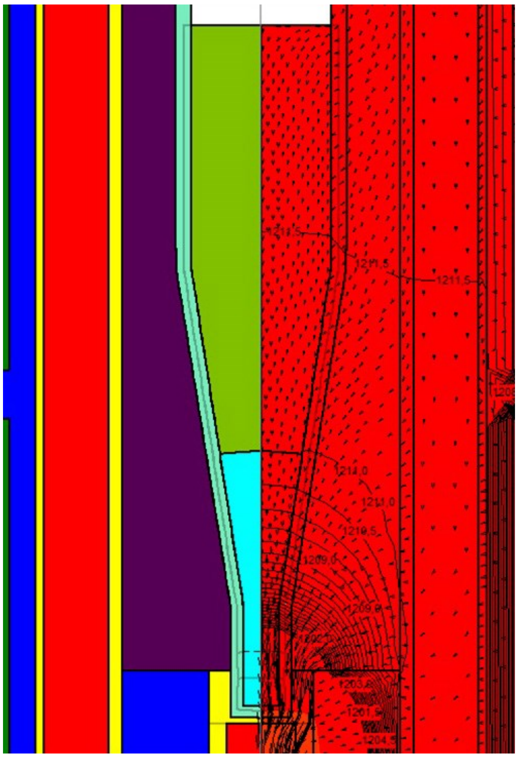

Fig. 4. The temperature field distribution inside the thermal unit.

On the developed configuration basis the four-zone furnace for the Bridgman-Stockbarger crystal growth technique with controlled heat exchanger was created, low radial and axial constant temperature gradients were obtained (Figure 5). The apparatus also allows to check the LGT crystal growth possibility in extremely low axial and radial temperature gradients.

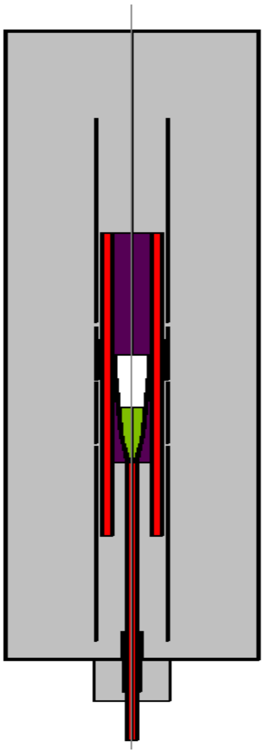

Fig. 5. The thermal unit construction

References:

1. Dash W.C. 1957. Dislocations and Mechanical Properties of Crystals. – N.Y.: Wiley
2. Indenbom V.L. 1957. Kristallografiya 2. – Moscow.: Nauka (in Russian)
3. Isaenko L. et al 2003. Growth and Properties of $LiGaX_2$ (X: S, Se, Te) Single Crystals for Nonlinear Optical Applications in the Mid-IR. – Cryst. Res. Technol.
4. Yelisseyev A. et al 2015. Spectroscopic properties of nonlinear optical $LiGaTe_2$ crystal. – Optical Materials
5. Wilke K.Th. 1973. Kristallzüchtung. – Berlin: VEB Deutscher Verlag der Wissenschaften

Korobova E.M.[1], Kolmykova L.I.[1], Gromyak I.N.[1], Korsakova N.V.[1], Makarova E.M.[2], Golubkina N.A.[3] Seasonal dynamics of iodine and selenium in natural water of different geochemical origin.

[1] V.I. Vernadsky Institute RAS, Moscow (korobova@geokhi.ru) [2] Geocentre “Bryansk”, Bryansk [3] VNIISSOK, Moscow

Abstract. Seasonal dynamics of iodine and selenium concentration has been studied in natural waters originating from various water-bearing complexes and horizons typical for Bryansk region (Russia). Obtained data proved a considerable seasonal variation in I and Se content ranging from 3,7 to 8,1 μg/l and 0,04-0,4 μg/l respectively. Variation was related to physico-chemical water parameters, such as pH, Eh and fluctuations in concentration of dissolved organic matter. The widest seasonal variation of the studied elements was observed in surface and well waters. Iodine maximum level was found in these waters in autumn (8,1 μg/l). Selenium content was higher in surface waters during summer-autumn period (0,06-0,3 μg/l) as compared to spring (0,04-0,05 μg/l). In drinking water from centralized supply pipeline low concentration of both elements was also registered in spring (3,7-4,3 μg/l (I) and 0,04-0,08 μg/l (Se)). Migration of iodine throughout the year occurs in fraction usually treated as dissolved (<0.45 μm) and the proportion of this fraction in autumn can reach its maximum equal to 84%.

Keywords: iodine, selenium, natural water, seasonal variation, Bryansk region

A large part of the territory of Russia belongs to biogeochemical provinces with a low content of iodine in the environment [Kovalsky V.V., 1974]. Insufficient intake of this element in the body leads to disruption of metabolic processes and formation of endemic diseases among the animals and humans [Fuge R., 1989]. Deficiency of other essential elements such as selenium may also have an influence on the occurrence of this kind of diseases [Rosen V. B., 1994].

Despite the accepted minor contribution of drinking water to providing living organisms with micronutrients [Fuge R., 2005], there are several regional studies which witness clear relationship between the amount of iodine in natural drinking waters and the occurrence of cases of iodine deficiency diseases among local population [Balasuriya S. et al., 1992; Salikhov Sh. K. et al., 2014.].

The Bryansk region belonging to non-chernozem zone is a clear example of areas with severe iodine deficiency in domestic animals due low I content in soils and food chains [Kovalsky V.V., 1974]. Iodine deficiency was registered among population and needed addition of I to diets [Dedov I.I. et al., 2006]. On the other hand, a considerable European part of this region has been affected by the Chernobyl accident (1986), and, as a result, it has been contaminated by radioactive isotopes including radioiodine. Under the condition of stable iodine deficiency radioactive iodine isotopes could have been accumulated by the I target organ, namely thyroid gland, more actively. The studies conducted after the accident proved contribution of iodine deficiency in humans to frequency of thyroid cancer cases in the contaminated zone [Shakhtarin V.V. et al., 2003]. Basing on the fact that rural diet is formed of local products and that vegetables contain ca 80% of water it could be suggested that contribution of water to local diet may reach 20% and it is worth to study peculiarities of I and Se migration of natural water in rural settlements contamination by radioiodine.

Our earlier studies of 2007-2013 showed wide iodine variation in natural waters of the region (0,74 - 41,19 μg/l) while surface and ground water samples were noted for the highest content of this element (8,4 μg/l, n=46 and 6,61 μg/l, n=52 respectively). Drinking water of centralized supply contained less iodine (6,39 μg/l, n=18). Similar character of distribution was observed for selenium. Its maximum level was detected in groundwater (0,53 μg/l, n=30) and water from centralized water supply (0,32 μg/l on the average, n=11). According to studies of water samples collected in previous years the levels of the trace elements depended on the overall chemical composition of the water (concentration of calcium, magnesium, sodium and potassium) and was related to salinity and Eh-pH parameters [Korobova E.M. et al., 2014 Kolmykova L.I., et al., 2016].

The aim of this study was to investigate seasonal dynamics of iodine and selenium concentration in natural waters fed by different water-bearing rocks resting at different depths.

The study was conducted in April-May, July and October of 2014-2015 at 14 monitoring points characterizing water sources connected to the uppermost layer (river and dug wells), the waters from drilled wells (ca 10-20 m deep) and centralized artesian bore holes draining geological strata down to 200 m. The highest content of iodine in surface and groundwater was observed in October (Me= 8,07 μg/l, n=3 in dug wells water and 5,12, n=5 in river and lake, average value for two seasons). A relatively high I concentration can be attributed to higher water salinity (Me=0,9 g/l), higher content of organic matter at the end of the growing season and more active leaching of iodine from soils sediments due to precipitation (Fig.1). Significant variations of iodine are observed for water from dug wells (5,10-8,07 μg/l); the water from drilled wells were characterized by the narrower range of its concentration (4,31-5,64 μg/l), the maximum being reached in July. Seasonal dynamics of Se content in natural waters was also quite obvious. The greatest seasonal range of Se values was found in dug well water (0,143-0,350 μg/l) where maximum was found in spring (Fig.2). In drilled and surface waters Se concentration varied in a smaller range, reaching maximum July (Me=0,067, n=6 for drilled wells and 0,056 μg/l, n=5 for rivers and lakes).

Analysis of the chemical composition of the filtrates obtained by passing the original water sample through a semipermeable membrane of cellulose acetate with pore size of 0,45 μm, showed a significant predominance of iodine in the soluble fraction, regardless of the season of the year (from 75% to 84%). As expected, the highest fraction of dissolved iodine was observed in autumn (84%) that corresponds to the total iodine maximum found in October (8,1 μg/l).

Therefore the minimum iodine uptake with water by organisms occurs in spring period (April-May) that may be an additional risk factor in case of an accidental release of radioactive iodine in this season of the year.

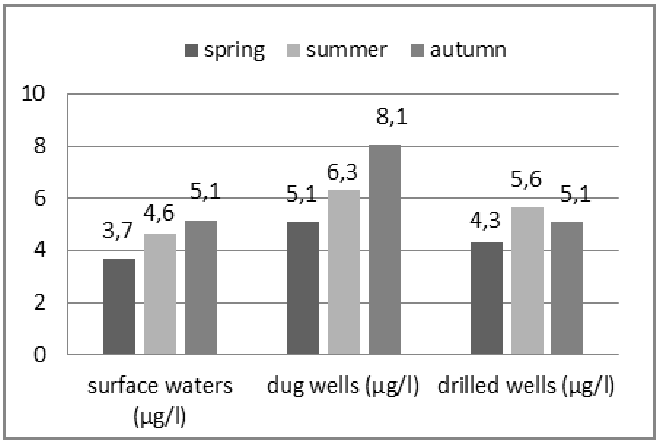

Fig. 1. The concentration of iodine (μg/l) in natural waters from different sources within a few seasons

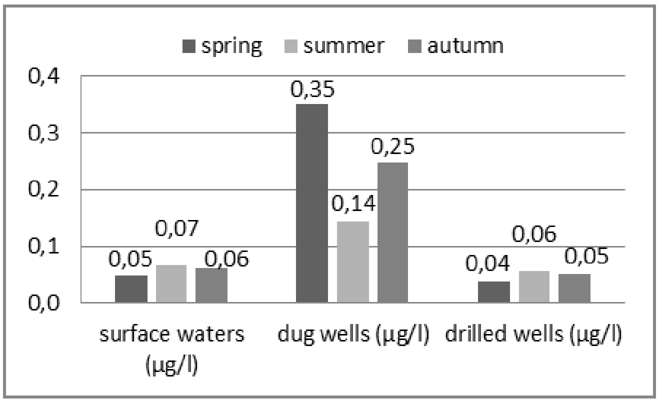

Fig. 2. The concentration of selenium (μg/l) in natural waters from different sources within a few seasons

The work was supported the Russian Foundation for Basic Research (grant 13-05-00823)

References:

1. Balasuriya S., Perera P.A.J., Herath K.B., Katugampola S.L. and Fernando M.A.. Role of iodine content of drinking water in the etiology of goitre in Sri Lanka. The Ceylon Journal of Medical Science. V. 35. 1992. P. 45-51.
2. Dedov I.I., Melnichenko G.A., Troshina N.M. et al. National report/ Ministry of Health and Social Development of the Russian Federation, , Endocrinologic Scientific Center of the Russian Academy of Sciences, Center for Iodine Deficiency Diseases, Institute of Nutrition, Center for Scientific-Technical Cooperation of Enterprises of Salt Industries. Moscow. 2006. 124 p. (in Russian).
3. Fuge R. Iodine in waters; possible links with endemic goitre. Applied Geochemistry. V.4. 1989. P. 203-208.
4. Fuge R. Soils and iodine deficiency// O. Selinus, B.J. Alloway, J.A. Centeno, R.B. Finkelman, R. Fuge, U. Lindh et al. (Eds), Essential of medical geology: Impacts of the natural environment on public health. 2005. P. 417-433.
5. Kolmykova, L.I., Korobova E.M., Ryzhenko B.N. The contents and features of the distribution of iodine in natural waters of the Bryansk region. Bulletin of Tyumen state University. Vol. 2. No 1. 2016. P.8-19 (in Russian).
6. Korobova E.M., Ryzhenko B.N., Cherkasova E.V., Sedykh E.M., Korsakova N.V., Danilova V.N., Khushvakhtova S.D., and Berezkin V.Yu. Iodine and Selenium Speciation in Natural Waters and Their Concentrating at Landscape–Geochemical Barriers. ISSN 0016_7029, Geochemistry International. 2014. Vol. 52. No. 6. P. 500–514. Pleiades Publishing, Ltd., 2014.
7. Kovalsky V.V. Geochemical ecology of endemic goiter /V. Kowalski, R.I. Blokhina // Problems of geochemical ecology of organisms. M. 1974. Vol. 13. P. 191-216 (in Russian).
8. Kovalsky V.V. Geochemical ecology. M., 1974, 282 p. (in Russian).
9. Rosen V.B. Principles of endocrinology. 3rd edition under the editorship of Dr. Biol. Sciences O. V. Smirnova. Moscow. 1994. 117 p. (in Russian).
10. Salikhov Sh. K., Yakhyaev M. A., S. G. Loginova, M. G. Ataev Z. V. Kurbanova, K. A. Alimetov. Endemic goiter in Dagestan as a result of deficiency of iodine and selenium in the objects of its biosphere. Bulletin of the TSU. Vol. 19. No. 5. 2014. P. 1729-1732 (in Russian).
11. Shakhtarin, V.V., Tsyb, A.F., Stepanenko, V.F., Orlov, M.Y., Kopecky, A.J., and Davis, S. Iodine deficiency, radiation dose, and the risk of thyroid cancer among children and adolescents in the Bryansk region of Russia following the Chernobyl power station accident // International Journal of Epidemiology. 2003. Vol.32. P. 584-591.

Osadchii Valentin O. [a,b] An experimental study of the solubility of Bi_2O_3 and Sb_2O_3 in H_2O vapor

[a] Faculty of Geology, M.V. Lomonosov Moscow State University, Moscow, 119991, Russia
[b] Institute of Experimental Mineralogy RAS, Chernogolovka, Moscow District, 142432, Russia
E-mail: v.osadchii@iem.ac.ru

Keywords: bismuth; antimony; water vapour; solubility;

Introduction

Bismuth and antimony are trace elements and their concentrations in the earths crust are usually less then 1 ppm. Nevertheless they are easily mobilized by hydrothermal fluid and can reach concentrations up to 100 ppm [1, 2]. In geological processes geochemistry of Sb is closely related to such elements as Ag, Ag and PGE, while Bi is known as a 'pathfinder' element for Au and can scavenge significant amounts of gold from host rocks [3]. Unfortunately there is a lack of the thermodynamic data for these elements which limits our understaning of their role in hydrothermal processes. Thus, since the solubility of Bi_2O_3 and Sb_2O_3 in dense water vapor is still unknown, the aim of these study was to measure the solubility of Sb_2O_3 and Bi_2O_3 in the water vapor in the systems Sb_2O_3-Bi_2O_3-H_2O at 330-360°C and *saturated water pressure*.

Materials

In our experiments we used distilled deionised water; crystalline bismuth oxide Bi_2O_3 (bismite) and crystalline antimony oxide (senarmontite) produced by Sigma-Aldrich.

Experimental and analytical techniques. Experiments were carried out in Ti-based (VT8) autoclave (90 cm^3) with an inner ampoule (6 cm^3) for *in situ* sampling of vapor phase. This technique is described in details elsewhere [4, 5]. The pressure during the runs was measured with a D100 strain gauge calibrated against a standard piston gauge. The autoclave temperature was monitored by the K-type thermocouple. The uncertainties in the pressure and temperature measurements are ±0.3MPa and 1K, respectively. The amount of Bi_2O_3 and Sb_2O_3 was at least two orders higher than its solubility in water at the temperature of experiment.

After heating for 2-3 days (which was enough for system to equilibrate) the inner capsule was opened for 5 minutes and then closed, the autoclave was removed from the oven and quenched in cold water. After quenching, the capsule containing condensed vapor was rinsed 8 times with a well-known quantity 3M HNO_3 solution. These wash solutions were collected and then analysed separately by the ICP method.

Results

The discrepancies between the measured temperature and pressure and the water saturation curve are within instrumental accuracy. The obtained solubility of Bi and Sb in vapor was used to calculate the partition between dense water solution [3, 6] and coexisting vapor. Results are presented in Fig. 1.

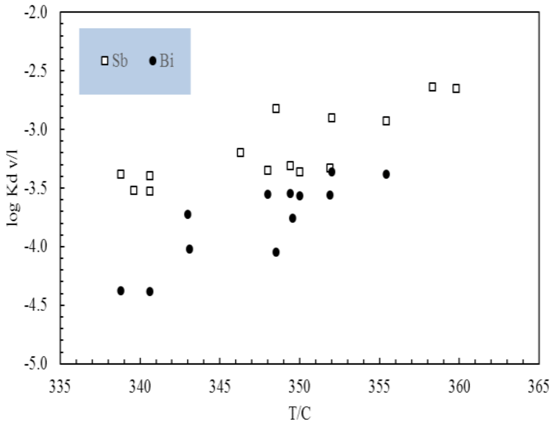

Fig. 1. The solubility of Bi_2O_3 and Sb_2O_3 in water vapor.

The research presented in this paper was funded by RSF (grant №14-17-00366 to N. Akinfiev). *I am grateful to Ya. V. Bychkova for conducting the ICP-MS analysis and A.V. Zotov for his comments on the experimetal part of this study.*

References:

1. Pokrovski GS, Borisova AY, Bychkov AY (2013) Speciation and Transport of Metals and Metalloids in Geological Vapors. Rev Mineral Geochemistry 76:165–218. doi: 10.2138/rmg.2013.76.6
2. Pokrovski GS, Borisova AY, Roux J, et al. (2006) Antimony speciation in saline hydrothermal fluids: A combined X-ray absorption fine structure spectroscopy and solubility study. Geochim Cosmochim Acta 70:4196–4214. doi: 10.1016/j.gca.2006.06.1549
3. Tooth B, Etschmann B, Pokrovski GS, et al. (2013) Bismuth speciation in hydrothermal fluids: An X-ray absorption spectroscopy and solubility study. Geochim Cosmochim Acta 101:156–172. doi: 10.1016/j.gca.2012.10.020
4. Zakirov IV, Sretenskaja NG, Aranovich LY, Volchenkova VA (2007) Solubility of NaCl in CO2 at high pressure and temperature: First experimental measurements. Geochim Cosmochim Acta 71:4251–4255. doi: 10.1016/j.gca.2007.01.028
5. Akinfiev NN, Zotov A V. (2016) Solubility of chlorargyrite (AgCl(cr./l.)) in water: New experimental data and a predictive model valid for a wide range of temperatures (273–873K) and water densities (0.01–1g·cm−3). Geochim Cosmochim Acta 178:178–194. doi: 10.1016/j.gca.2016.01.027
6. Zotov A.V., Shikina ND, Akinfiev NN (2003) Thermodynamic properties of the Sb(III) hydroxide complex Sb(OH)3(aq) at hydrothermal conditions. Geochim Cosmochim Acta 67:1821–1836. doi: 10.1016/S0016-7037(00)01281-4

Zakirov[a] Ildar V., Suvorova[a] Valeria A.*, Osadchii[a,b] Valentin O. An experimental study of the solubility of tin in H_2O vapor

[a] Institute of Experimental Mineralogy RAS,
Chernogolovka, Moscow District, 142432, Russia

[b] Faculty of Geology, M.V. Lomonosov Moscow State University, Moscow, 119991, Russia
* lera@iem.ac.ru

Keywords: tin; water vapour; solubility; cassiterite;

Introduction

The behavior of tin in hydrothermal geological processes is primerily controlled by the solubility of cassiterite [1]. In chlorine-free environment tin is usually present in the form of either $Sn(OH)_2$ or $Sn(OH)_4$ in both aqueous solutuions and water vapor. The thermodynamic parameters of the former are well-studied [2], while the properties of the latter are still unknown. For this reason we conducted experimental studies of cassiterite solubility in water vapor in the system SnO_2-H_2O at 330-360°C and *saturated water pressure*.

Materials

In our experiments we used distilled deionised water and crystalline tin oxide SnO_2 produced by Sigma-Aldrich.

Experimental and analytical techniques. Experiments were carried out in Ti-based (VT8) autoclave (120 cm^3) with an inner ampoule (19.2 cm^3) for *in situ* sampling of vapor phase. This technique is described in details elsewhere [3, 4]. The pressure during the runs was measured with a D100 strain gauge calibrated against a standard piston gauge . The autoclave temperature was monitored by the S-type thermocouple. The uncertainties in the pressure and temperature measurements are ±0.3MPa and 2K, respectively. The amount of SnO_2 was at least two orders higher than its solubility in water at the temperature of experiment.

After heating for 2-3 days (which was enough for system to equilibrate) the inner capsule was opened for 5 minutes and then closed, the autoclave was removed from the oven and quenched in cold water. After quenching, the capsule containing condensed vapor was rinsed 8 times with a well-known quantity 3M HNO_3 solution. These wash solutions were collected and then analysed separately by the ICP method.

Table 1. The solubility of SnO_2 in saturated water vapor

№	T, °C	Sn, ppb
18	330	2356
19	330	3204
21	350	4785
22	350	4008
23	350	3811
24	360	5001
25	360	5913
26	360	5906

Results

The discrepancies between the measured temperature and pressure and the water saturation curve are within instrumental accuracy. The measured solubility of cassiterite is shown at table 1 and figure 1 and at least one order higher than its solubility in aquoeus water solution measured by Sorokin and Dadze [5]. Thus, the solubility of SnO_2 in water needs to be re-examined.

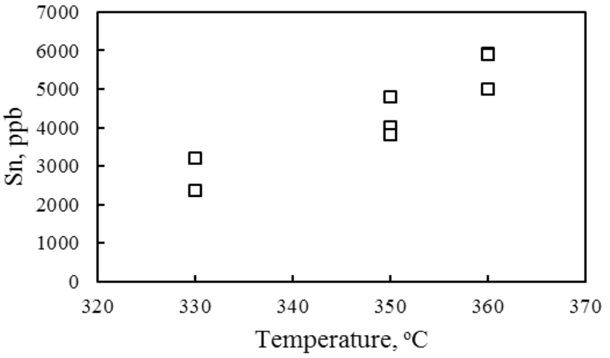

Fig. 1. The solubility of SnO_2 in water vapor

The research presented in this paper was funded by RSF (grant №14-17-00366 to N. Akinfiev). *We are grateful to Ya. V. Bychkova for conducting the ICP-MS analysis and A.V. Zotov for his comments on the experimetal part of this study.*

References:

1. Migdisov AA, Williams-Jones AE (2005) An experimental study of cassiterite solubility in HCl-bearing water vapour at temperatures up to 350 °C. Implications for tin ore formation. Chem Geol 217:29–40. doi: 10.1016/j.chemgeo.2004.11.018
2. Cigala RM, Crea F, De Stefano C, et al. (2012) The inorganic speciation of tin(II) in aqueous solution. Geochim Cosmochim Acta 87:1–20. doi: 10.1016/j.gca.2012.03.029
3. Zakirov IV, Sretenskaja NG, Aranovich LY, Volchenkova VA (2007) Solubility of NaCl in CO_2 at high pressure and temperature: First experimental measurements. Geochim Cosmochim Acta 71:4251–4255. doi: 10.1016/j.gca.2007.01.028
4. Akinfiev NN, Zotov AV. (2016) Solubility of chlorargyrite (AgCl(cr./l.)) in water: New experimental data and a predictive model valid for a wide range of temperatures (273–873K) and water densities (0.01–1g·cm−3). Geochim Cosmochim Acta 178:178–194. doi: 10.1016/j.gca.2016.01.027
5. Sorokin VI, Dadze TP (1994) Solubility and complex formation in the systems Hg-H_2O, S-H_2O, SiO_2-H_2O and SnO_2-H_2O. Fluids in the Crust. Springer Netherlands, Dordrecht, pp 57–93

Polotnyanko N.A.[1], Tyurin A.V.[2], Kristavchuk A.V.[3], Chareev D.A.[3], Gavrichev

K.S.[2] Heat capacity and thermodynamic properties of palladium sulfides

1-Dubna University; 2- IGIC RAS; 3- IEM RAS
polot.nat@gmail.com

The present work is a continuation of complex research focused on thermodynamic properties of the inorganic compounds containing palladium, in particular, included in S-Pd system. To date, literature data related to above-mentioned system is severely lacking.

Palladium forms several sulfides. Among these sulfides there are such minerals as vysotskit PdS and vasilit $Pd_{16}S_7$. Synthetic analogs of natural vysotskit and vasilit were obtained by solid-state synthesis. Samples were characterized by means of X-ray analysis.

Calorimetric measurements of heat capacity of palladium sulfides in a wide temperature range are given. Standard thermodynamic functions for both phases were calculated.

UDC 550.424.6

Aleksandrova E.V. Modeling of colloidal particles sorption on country rocks.

IGEM RAS, Moscow (ligasmy@gmail.com).

Abstract. Colloidal form - is the most dangerous form of radionuclides migration in underground environment. According to traditional models, radiocolloid sorption is considered as initial deposition on the free surface of enclosing rocks. As an alternative model has been proposed that takes into account the presence previously adsorbed non-radioactive colloid particles on the surface of filtration channels. Calculations on the basis of both models have shown that the intensity of colloidal particles precipitation depends on the number K_L, which characterizes the ratio of groundwater velocity to desorption rate of colloidal particles.

Key words: radionuclides, groundwater, radiocolloid, deposition.

The main way of radionuclide migration in the underground environment in case of leakage from the territory of the storage of radioactive waste is the transfer by groundwater. Speed of radionuclide migration depends on the form of radionuclide transport in the underground environment. It was found that the most mobile form is a colloidal form of transport (Penrose et al., 1990; Kersting et al., 1999; Airey P.L., 1986; Short S.A., Lowson R.T., 1998).

Methods of mathematical modeling are used to assess the rate of radionuclide migration in colloidal form. Existing models of radionuclide transport in the underground environment take into account only radionuclide deposition on the free surface of the enclosing rocks. In this case radiocolloids (radionuclides are carried in colloidal form) occupy all adsorption space when passing front of radioactive contamination. As a result of decreased speed of radioactive contamination in the underground environment (*Model I*).

In practice radiocolloid deposition is a substitution of previously deposited particles - non-radioactive particles of natural origin (*Model II.*). Of particular interest is the analysis of calculation results is made by using the *Model I* and *Model II.* Two options of radioactive contamination spread in underground environment are possible:

1. The groundwater flow rate is much higher than the rate of desorption of non-radioactive colloid particles from the surface of filtration channels. This condition is met for small values of K_L (K_L = 0.1). In this case, the distribution of dimensionless radiocolloid concentration over the entire length of the contamination front can be represented in the form of curves are shown in *Fig. 1,2*.

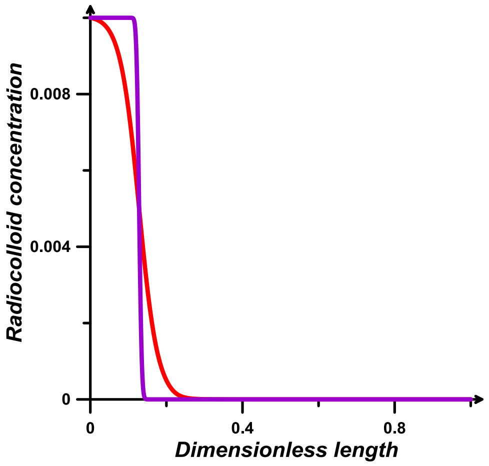

Fig. 1. Distribution of dimensionless radiocolloid concentration in the groundwater along the length of the rock at ϑ= 0.2 (ϑ - the dimensionless time; K_L=0.1)

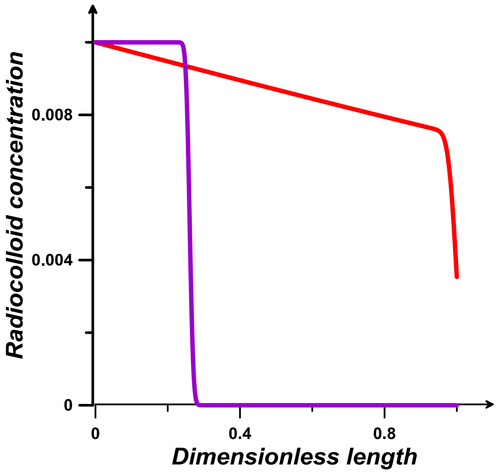

Fig. 2. Distribution of dimensionless radiocolloid concentration in the groundwater along the length of the rock at ϑ= 1 (ϑ - the dimensionless time; K_L=0.1)

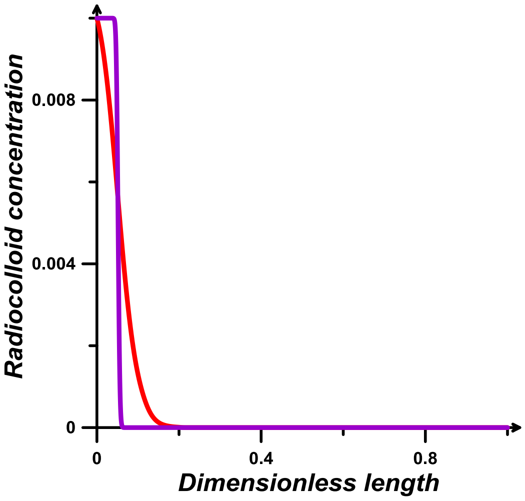

Fig. 3. Distribution of dimensionless radiocolloid concentration in the groundwater along the length of the rock at ϑ= 0.2 (ϑ - the dimensionless time; K_L=10)

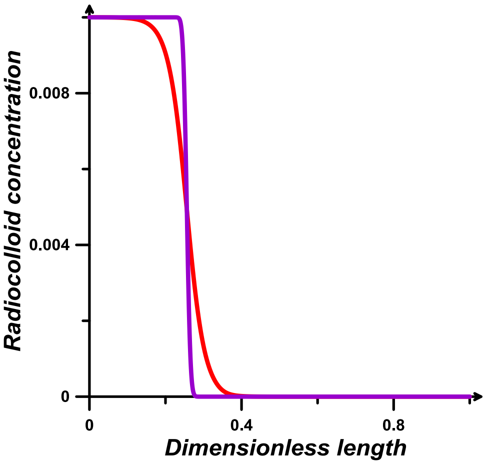

Fig. 4. Distribution of dimensionless radiocolloid concentration in the groundwater along the length of the rock at ϑ= 1 (ϑ - the dimensionless time; K_L=10)

Fig. 1 – 4: red curves show the results of calculations made on the basis of the *Model II*, purple curves - *Model I.*

The calculations show that for small values of K_L in the case of *Model II* front of radioactive contamination spreads much faster than in the case of using of *Model I.*

2. The rate of groundwater flow is much smaller than desorption rate of previously precipitated colloid particles of natural origin. This condition is met for large values of K_L ($K_L = 10$). Curves presented in *Fig. 3.4*, show that in this case the differences in results on the basis of *Models I* and *II* are minimal.

New model has been proposed. This model takes into account the presence of previously adsorbed non-radioactive colloid particles on the surface of filtration channels. Conducted research have shown the relevance of the proposed model in the calculation of radioactive contamination spread in underground environment.

References:

1. Airey P.L. Radionuclide migration around uranium ore bodies in the Alligator Rivers region of the northern territory of Australia – analogue of radioactive waste repositories – a review // Chemical Geology. – 1986. – V. 55. – № 3. – P.255–268.
2. Kersting A.B., Efurd D.W., Finnegan D.L., et al. Migration of plutonium in ground water at the Nevada Test Site // Nature. – 1999. – V. 397. – P.56–59.
3. Penrose W.R., Polzer W.L., Essington E.H., Nelson D.M., Orlandini K.A. Mobility of plutonium and americium through a shallow aquifer in a semiarid region // Environmental Science & Technology. – 1990. – V. 24. – № 2. – P. 228–234.
4. Short S.A., Lowson R.T. 234U/238U and 230Th/234U activity ratios in the colloidal phases of aquifers in lateritic weathered zones // Geochimica et Cosmochimica Acta. – 1988. – V.52. – N.11. – P. 2555–2563.

Bublikova T.M., Balitsky V.S. Experimental Determination of the Heat Capacity of Basic Copper Carbonates (Malachite and Azurite)

IEM RAS, *Chernogolovka* (tmb@iem.ac.ru, balvlad@iem.ac.ru)

Abstract. The experimentally determined heat capacity of basic copper carbonates: natural malachite $CuCO_3$ $Cu(OH)_2$ and azurite $2CuCO_3$ $Cu(OH)_2$ and malachite synthesized in IEM RAS. The obtained data were used to calculate the thermodynamic functions of these minerals. Experimental results and theoretical calculations were used for the solubility diagrams in the system copper compounds CuO-CO_2-H_2O-NH_3 at a different temperature and ammonia concentration.

Keywords: malachite, azurite, copper carbonate, heat capacity

Phase relations in the system CuO-CO_2-H_2O-NH_3 were studied to determine the stability of the fields and the conditions of crystallization of malachite and azurite in copper-carbonate systems. We calculate and build diagrams of solubility of copper compounds at temperatures up to 100°C and a pressure of 0.1 MPa for various ammonia concentrations using some data in the literature.

In the literature, there are estimates of the heat capacity of malachite and azurite [Helgeson et al., 1978], as well as experimental data on the nature of basic copper carbonate [Kiseleva et al., 1992]. For the most accurate and concerted thermodynamic characteristics we measured the heat capacity of malachite synthesized in IEM RAS [Balitsky V.S., Bublikova T.M. et al., 1987] and natural samples of malachite and azurite.

Dependencies of the heat capacity on the temperature, obtained by us experimentally, were used to calculate the thermodynamic functions of basic copper carbonates.

Heat capacity measurement was conducted with a differential scanning calorimeter DSC-2 «Perkin-Elmer» in an atmosphere of pure argon at a heating rate of 20 K/min, using the comparison method.

To reduce the thermal drift calorimeter held for one hour at a temperature of 1000 K. The samples synthetic sapphire with different masses were used as reference of heat capacity.

The output signal of the calorimeter was entered into the computer memory via an analog-to-digital converter. After baseline correction form on these calculation data held in the sample heat capacity versus temperature. Error determination of the heat capacity does not exceed 2%, and the reproducibility was better than 5%.

Measurements were carried out in two stages: at 260 - 340 K and 360 - 500 K. The samples: natural malachite (mine Chokpak, Kazakhstan), azurite (copper-sulphide deposits in the Urals, a sample of the Mineralogical Museum VNIISIMS) and synthetic malachite, resulting in a crystallizer recirculating type IEM RAS. The measured values of C_p^o accepted as the phase with perfect stoichiometry due to the lack of satisfactory data on the composition of samples of azurite.

Temperature dependence of the heat capacity of natural malachite and azurite and malachite synthetic shown in Fig. 1 and 2.

Dependence of the heat capacity - temperature (298.15 - 500 K; J/mol K): were obtained by treating the measurements by method of least squares:

natural malachite:

$C_p^o = 88.77 + 254.59 \cdot 10^{-3}T - 9.27\ 10^5 \cdot T^{-2}$

synthetic malachite:

$C_p^o = 66.26 + 331.80\ 10^{-3}T - 3.02 \cdot 10^5 \cdot T^{-2}$

natural azurite:

$C_p^o = 102.70 + 451.84\ 10^{-3}T - 7.30\ 10^5 \cdot T^{-2}$

The calorimetric data indicate that synthetic malachite heat capacity on average 4% higher than the heat capacity of the natural malachite. The reasons for this difference may be: lower crystallinity the synthetic sample, a higher content of volatile components, as well impurities trapped into the sample during synthesis.

Fig. 1, 2 also shows the dependence of the heat capacity of the temperature by H. Helgeson [Helgeson H.C. et al., 1978]. He calculated the equation of the temperature dependence of malachite and azurite, based by his method, called "structural algorithm."

It should be noted a good agreement between the experimental and estimated values: the maximum difference of 7% noted for malachite at 260 K and 10% for azurite at 260 K.

For the calculation of the thermodynamic functions of malachite and azurite at high temperature our experimental C_p^o equations were used.

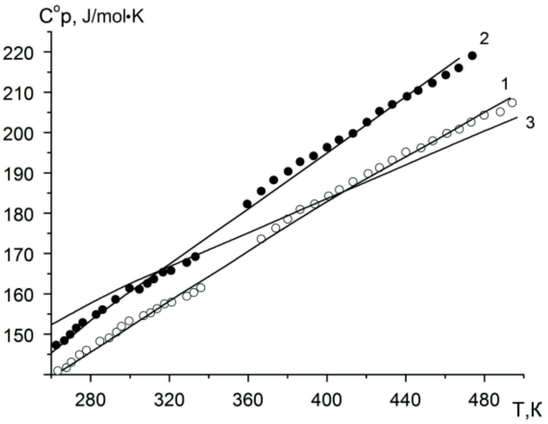

Fig. 1. Temperature dependence of the heat capacity: 1 - natural malachite, 2 - synthetic malachite, 3 - malachite by Helgeson H.C. et al., 1978.

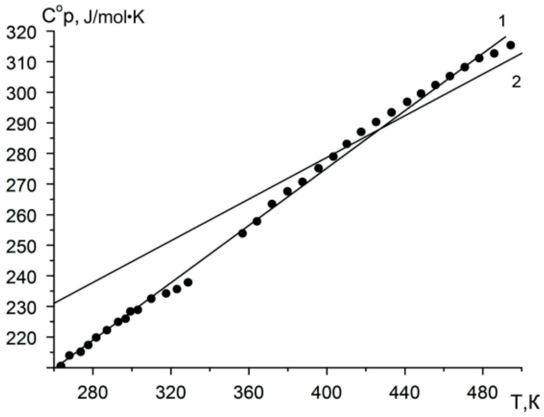

Fig. 2. Temperature dependence of the heat capacity: 1 - natural azurite, 2 - azurite by Helgeson H.C et al., 1978.

The standard enthalpies of formation of malachite (-1058.57 kJ·mol^{-1}) and azurite (-1663.20 kJ·mol^{-1}) calculated on the basis of our experimental data show good agreement with the values $\Delta_f H^o_{298.15}$ for malachite and azurite in [Preis, Gamsjäger, 2002] devoted to detailed review and analysis of thermodynamic data for the basic copper carbonates.

References:

1. Balitsky V.S., Bublikova T.M., Sorokina S.L. et al. Man-made jewelry malachite. Gems and Gemology. 1987.V. 23. P. 152 – 157.
2. Helgeson H.C., Delany J.M., Nesbit H.W. et al. Summary and critique of the thermodinamic properties of rock-forming minerals. 1978. Am.J.Sci.1978.V. 278A: 1-229.
3. Kiseleva I.A., Ogorodova L.P., Melchakova L.V., Bisengalieva M.R., and Becturganov N.S. Thermodynamic Properties of Copper Carbonates – Malachite $Cu_2(OH)_2CO_3$ and Azurite $Cu_3(OH)_2(CO_3)_2$. Phys. Chem. Minerals. V. 19. P. 322-333.
4. Preis W, Gamsjäger. Solid–solute phase equilibria in aqueous solution. XVI. Thermodynamic properties of malachite and azurite—predominance diagrams for the system Cu^{2+} – $H_2O–CO_2$. 2002 J. Chem. Thermodynamics. V. 34.P. 631–650.